Tissue Welding: Studies of Pulsed Diode Laser Interaction with ICG Stained Porcine Aorta and Elastin-Based Biomaterial

Elaine Naomi La Joie
B. S. San Jose State University, 1992

A thesis submitted to the faculty of the
Oregon Graduate Institute of Science & Technology
in partial fulfillment of the
requirements for the degree
Master of Science
in
Applied Physics

July 1995

The thesis "Tissue Welding: Studies of Pulsed Diode Laser Interaction with ICG Stained Porcine Aorta and Elastin-Based Biomaterial" by Elaine Naomi La Joie has been examined and approved by the following Examination Committee:

Scott A. Prahl
Assistant Professor
Thesis Research Adviser

Kenton Gregory
Director, Oregon Medical Laser Center

Anthony Bell
Associate Professor

Acknowledgements

I would like to acknowledge the Oregon Medical Laser Center and Dr. Ken Gregory for providing lab, equipment and support. I thank Andrew Barofsky for providing and perfecting the biomaterial, Ujwal Sathyam for aligning and setting up the photothermal radiometer. I would especially like to thank Dr. Scott Prahl for his encouragement and guidance. And, I would like to acknowledge the National Institutes of Health, and its MARC predoctoral fellowship (Grant number GM15461-02) for supporting me during this research.

Contents

List of Tables

List of Figures

Abstract

Tissue Welding:
Studies of Pulsed Diode Laser Interaction
with ICG Stained Porcine Aorta
and Elastin-Based Biomaterial

Elaine Naomi La Joie, M.S.
Oregon Graduate Institute of Science & Technology, 1995

Supervising Professor: Scott A. Prahl

Laser tissue welding is a sutureless method of wound closure that has been used successfully in nerve, skin, and arterial anastomoses. After heating generated by laser exposure, a glue is formed between tissue edges that forms a weld upon cooling. The advantages of laser welding over traditional wound closure are no foreign body reaction and less scar formation. However, traditional methods of laser welding have a minimal surface area of tissue to weld, such as in anastomoses. Also, excess heating occurs with the use of traditional surgical CW lasers such as the Argon and CO_2. These studies used an artificial biomaterial made mostly of elastin and fibrin to weld to porcine aorta, which allowed greater surface area for welding and measurement of optical properties of the weld site. Also, a pulsed diode laser was used to maintain thermal confinement and therefore minimize excess heating.

Steady state thermal experiments indicated that the elastin-based biomaterial was thermally stable up to 100°C. Welds between biomaterial and aorta were successful between 65–80°C with pressures of $5\,\mathrm{N/cm^2}$ for immersions of 5 minutes.

Photosensitive dyes with high absorption at the laser wavelength are added to the weld site to increase heating and to minimize thermal damage to surrounding unstained tissue. The intimal

surface of porcine aorta was stained with indocyanine green dye to efficiently absorb 808 nm diode laser light. A 5 mg/ml solution of indocyanine green dissolved in water penetrated 200 μm into the intimal side of porcine aorta.

Transmission measurements of stained aorta were made using radiant exposures of 6–129 mJ/mm^2 and using pulse durations of 0.5–5 ms. Transmission increases and reaches a maximum of 80–85% with successive pulses for radiant exposures greater than $\sim$25 mJ/mm^2, indicating that the absorption coefficient, and therefore heating, of stained tissue decreases with repetitive pulses.

Thermal measurements of the surface of stained aorta using a photothermal radiometer were made for radiant exposures of 38–120 mJ/mm^2. Temperature rises of 10–100°C were measured after one pulse. Thermal measurements of samples from different aortas, each stained with new solutions of ICG, showed the wide variability in the heating of tissue, and therefore the variability in concentration of ICG for different samples.

Simultaneous transmission and thermal measurements were made of stained aorta to eliminate sample variability and to compare the absorption coefficients calculated from each measurement. As in previous transmission measurements, transmission increased over pulses, indicating a decrease in absorption. However, the surface temperature, and therefore the absorption coefficient remained constant over repetitive pulses. It was postulated that ICG was undergoing a photochemical change with repeated exposure to laser light. This change was thought to be a change in effective depth of the ICG since the penetration depth of ICG was the only hard to measure quantity in our calculations. The effective depth of stain is inversely proportional to the fourth root of the pulse number.

Laser welds of stained aorta to biomaterial were attempted by sandwiching the samples between glass slides and applying pressures ranging from 4–20N/cm^2 for 5 ms pulse durations and 86 mJ/mm^2 radiant exposure. Welds were successful for pressures above 11 N/cm^2.

Chapter 1

Introduction

Laser tissue welding is the process of uniting or fusing two pieces of tissue with a laser. Upon cooling, a bond is established between tissue edges. Tissues that have been successfully welded include gallbladder, intestine and artery [1–3]. The advantages over traditional suture and staple methods are no foreign body reaction, less scar formation, no leakage due to suture holes, and shorter operating times [4]. The greatest disadvantage is that the mechanism is poorly understood, resulting in confusion over the ideal parameters for welding. It is not known if the mechanism varies for different types of tissue, laser wavelengths, and temperature at the weld site. Finally, the success of the weld is operator dependent — one surgeon may develop a technique that cannot be replicated by another surgeon.

1.1 History

1.1.1 Laser Tissue Welding

The first laser welds were made with commonly available surgical lasers such as CO_2 argon, and Nd:YAG lasers. Tissue, which is mostly composed of water, strongly absorbs CO_2 laser energy, and has a penetration depth of about $10\,\mu$m [5]. The CO_2 laser has been used for microvessel anastomoses, nerve anastomoses, and joining skin [5–7]. Welding medium and large sized arteries (3–5 mm in diameter) was unsuccessful because the laser light did not penetrate sufficiently deep into the artery. The resulting welds could not withstand systolic blood pressure, and significant thermal damage is found in collateral tissue [3, 6].

The argon laser, with moderate tissue penetration of about $200\,\mu$m, successfully welded medium and large sized arteries, and created vein–artery anastomoses [8]. White *et al.* claimed that the mechanism for welding was crosslinking since the temperatures required for good welds

were between 43–48°C [9]. Brooks *et al.* later refuted this, stating that welds occurred around 100°C [10]. Fujitani *et al.* found that weld strength depended on a physiobiochemical bond in annealing collagen, and thus a precise positioning of tissue edges is required [11].

The Nd:YAG laser successfully welded medium sized artery anastomoses in the 95–115°C range, but the welds tended to be constricted, leading to a loss in elasticity [10]. This is undesirable in a vessel that must be free to expand and contract with blood flow. Large artery welds failed after 20–40 minutes [9]. In studies by Jenkins *et al.* the Nd:YAG laser was used to weld disturbed plaque to aorta in an attempt to simulate smoothing the vessel wall following balloon angioplasty [12]. A temperature range of 95–140°C was needed to obtain effective welds. No appreciable welds were achieved below 80°C, and charring occurred above 150°C [12].

1.1.2 Possible Mechanism

To pinpoint the mechanism of laser welding, steady-state welds were performed in a water bath. Solhpour *et al.* found that optimal welds between bovine Achilles tendon were achieved with pressures of 14.7 N/cm^2 and within 58–62°C [13]. Birefringence of collagen was present in all cases of strong welds, but Anderson *et al.* discovered that at the point of contact between tissue edges, collagen fibers lost their birefringence [14]. Anderson *et al.* suggested that heat generated by the laser melts unravelled collagen fibrils to form a glue [14]. These studies indicate that collagen plays a major role in the mechanism of tissue welding.

1.1.3 Thermal Confinement

Laser tissue welding is primarily a thermal process. Therefore, understanding heating of the weld site is critical to achieving successful welds. Jacques defined the optical zone as the depth at which the fluence has dropped to 35% of the original radiance [15]. Thermal confinement means that thermal diffusion is too slow to diffuse out of the optical zone. Achieving thermal confinement while welding is essential to minimizing collateral thermal damage. Thermal confinement is achieved at pulse durations shorter than

$$t = d^2/\kappa$$

where κ is the thermal diffusivity of the tissue, d is the thickness of the absorbing layer, and t is the duration of the laser pulse [15]. In the case of welding stained tissue with a d of 200 μm, thermal confinement is maintained with pulse durations less than 285 ms. The laser source in

these studies is an 808 nm pulsed diode laser with a pulse length of 1–5 ms, much shorter than 285 ms.

1.1.4 Photosensitive Dyes and Glues

Light absorbing dyes are applied directly to weld sites to reduce thermal damage to surrounding tissue, because the stained area has a higher absorption coefficient than the unstained surrounding tissue. These dyes usually have absorption peaks that match the wavelength of the laser used. The energy required for a successful weld is reduced because light is strongly absorbed by the dye. The strong absorption localizes heating to the stained area.

Fluorescein isothiocynate (FITC) has a peak absorption at 495 nm, close to the 488 nm emission line wavelength of the argon laser. Chuck *et al.* found that using FITC and the argon laser to weld rabbit aorta required less laser power than welding without FITC. They noticed that the presence of blood was helpful in making strong welds [16].

Oz *et al.* used indocyanine green (ICG) with a maximum absorption at 805 nm and a diode laser with a wavelength of 808 nm to weld abdominal rabbit aorta Figure 2.4 Welds could only be achieved using the dye [17]. DeCoste *et al.* used ICG and a tunable alexandrite laser operated at 780 nm to weld guinea pig skin. They found that ICG stained collagen at the wound edges, which served to keep dye in the desired location for welding. Welds were significantly stronger with ICG than without ICG [7].

Despite the promise of photosensitive dyes, welding still required stay sutures to precisely align tissue edges to weld anastomoses and fistulas, and to stabilize the initially weak welds*. To alleviate these problems, glues and absorbable stents were developed. Grubbs *et al.* used fibrinogen glue to weld microvessel anastomoses with the CO_2 laser. The glue consisted of fibrinogen, which is a clotting agent in blood, calcium ions, and thrombin [18]. Oz *et al.* used fibrinogen glue mixed with ICG to increase the weld strength of rabbit aorta welds [17]. The glues held the tissue together long enough for healing to occur before being reabsorbed into the body; however, fibrinogen glues are inconvenient to use, mainly because the fibrinogen must be collected from human blood, possibly exposing the patient to hepatitis and AIDS infection. Recently Bass *et al.* developed a healon-albumin solder that can be doped with ICG [19].

Similarly, absorbable stents act as a temporary frame over which healthy tissue may grow. Sauer *et al.* used a water soluble, absorbable stent, PolySurge, to weld the first sutureless bowel

*A fistula is a connection between juxtaposed veins or arteries

anastomosis with the Nd:YAG laser and India ink as the chromophore [20].

1.2 Background on Biomaterial

During blood clot formation, fibrinogen reacts with calcium ions and thrombin to form fibrin monomers and fibrinopeptides. The reaction progresses to form soluble fibrin, insoluble fibrin, and finally clot. Rabaud *et al.* discovered that soluble fibrin formed an adduct with elastin when thrombin and calcium ions were present [21].

Aprahamian *et al.* used this result and constructed an elastin–fibrin biomaterial [22]. The major constituents were the components of the original reaction — elastin, fibrinogen, thrombin, and calcium ions. Fibronectin was added to give the material more of a membrane like appearance. Including type I collagen added strength and did not interfere with the elastin–fibrinogen reaction as long as the ratio of elastin to collagen was around 100 to 1 [22]. Thiorea acted as a crosslinking agent, improving tensile strength. Rabaud *et al.* developed a elastin-collagen stent that was sutured into the stomach and the bladder and dissolved with six months with no scar formation [23].

Fradin *et al.* formed the resulting biomaterial into patches using Vicryl polyglactin as a lattice [24]. These patches were sewn into the intestinal tracts of pigs and humans, and seemed to prevent leakage into the abdomen [25]. The patch was sewn into rabbit aorta with no evidence of thrombus, inflammation or rejection, and the patch was completely absorbed [26]. The patches were shown to have good biocompatibility in the rat when sewn onto connective tissue, muscle, nerve, bladder, kidney, spleen, liver and peritoneum. The only non-compatible tissue tried was bone marrow [27].

1.3 Motivation for this work

Even though tissue welding has been studied for the past ten years, it has yet to gain wide acceptance in clinical use due to the many variables and unknowns of laser tissue welding. The pulsed 808 nm diode laser along with ICG may have practical advantages over other laser–dye combinations because the laser is small, low power, relatively inexpensive, and has a simple delivery system. ICG was used in cardiac output studies and has an 780–805 nm absorption peak in tissue that matches available diode laser emission wavelengths [7].

The pulsed nature of our laser may prevent excess heating and thermal damage to tissue.

The pulse lengths available are well below the pulse durations required for thermal confinement — all the laser energy is delivered before any begins to diffuse away.

Before welding *in vivo*, the mechanism of welding must be better understood. One factor that increases the difficulty of traditional welding attempts such as anastomoses and closing gaps in skin is the awkwardness of juxtaposing the tissue edges. Precise positioning is required. By welding biomaterial directly on top of aorta, it is not as critical to have edges exactly touching (such as in laser welding skin) since the top biomaterial layer will seal all gaps. The biomaterial may also be used to close holes in intestine. It is much easier to determine heating and transmission of light through the weld site with this geometry since there is more surface area to be welded. Since welding takes place at the interface between the biomaterial and the tissue (in our case, the ICG stained layer of the aorta) we studied the thin ICG layer as it was exposed to laser light.

Rabaud's elastin–based biomaterial was used as the absorbable patch. This patch has been used *in vivo* with no indication of rejection or infection [24]. Gregory and Grunkmeier at the Oregon Medical Laser Center laser welded a prototype elastin biomaterial using ICG as the chromophore. However, this material has not been laser welded with a pulsed diode laser. This project studies the feasibility of welding elastin based biomaterial to the aorta using the pulsed diode laser and ICG.

Chapter 2

Materials and Methods

2.1 Biomaterial

The elastin-based biomaterial was originally developed by Rabaud *et al.* who discovered adduct formation between elastin and fibrin [21]. By exploiting this adduct formation he formed a biomaterial that could be shaped into tubes or sheets, or directly molded onto a Vicryl lattice*. Rabaud claimed that the biomaterial was strong enough to act as a barrier to bacteria and as a scaffolding for regular cell growth [24]. I used this biomaterial without the lattice because of its elastic properties and reported encouraging results *in vivo* from Rabaud's group [27]. The protocol is similar to the latest method of Rabaud's for generating biomaterial [23].

2.1.1 Biomaterial Recipe

To make the biomaterial, insoluble elastin from bovine neck ligaments (Sigma) was shaken through a 40 μm fine mesh†. Next 280 mg of filtered insoluble elastin was swollen in an excess of phosphate buffer‡. The mixture was vortexed, centrifuged, and the excess buffer discarded. The swollen elastin was dissolved in 2 ml of phosphate buffer; 2 mg of collagen was dissolved in 0.6 ml of phosphate buffer; and 67 mg of fibrinogen (Sigma) was dissolved in 1 ml of phosphate buffer. These solutions were mixed together and held at 37°C in a water bath while thrombin and thiorea were prepared. Next, 200 μL of 14 mg/ml thiorea solution was added. A thrombin solution was prepared and kept on ice§. Since thrombin initiated the reaction, 0.2 ml of the thrombin solution

*Vicryl is the brand name of a suture thread with the properties of little foreign body reaction. Used in lattice form, it has the same purpose as reinforcing steel has when laying concrete.

†Smaller particles make a more homogeneous biomaterial.

‡The buffer contained in one liter of water, 0.103 g of $NaH_2{\cdot}4H_2O$, 0.035 g of Na_2PO_4, 0.203 g of $MgCl_2{\cdot}1H_2O$, 0.147 g of $CaCl_2{\cdot}1H_2O$, and 8.76 g of NaCl.

§175 units active thrombin in 1 ml of dionized water

was added last to 3.8 ml of the elastin mixture, and the mixture quickly poured into molds before it could harden. The molds were immersed in the 37°C water bath for 30 minutes.

The biomaterial was formed into 1 mm thick patches approximately 7×3 cm in area. Immediately after completion, the biomaterial had an opaque yellow appearance, almost like a wet, flat noodle. The biomaterial was elastic and did not deform with handling unless squeezed tightly between tweezers. The biomaterial was stored in 33% ethanol solution at 4°C. One hour before use it was transferred to a 0.9% saline solution at room temperature, and 15 minutes before use the biomaterial was transferred to fresh saline solution.

2.1.2 Progression of Recipe

Originally, I used soluble elastin in the biomaterial. Soluble elastin based biomaterial has the advantage of transparency, or a lower scattering coefficient which means less loss of laser light travelling through the biomaterial to the weld site when welding. However, the soluble elastin–biomaterial was neither as strong nor as elastic as insoluble elastin–based biomaterial. For this reason I switched to insoluble elastin-based biomaterial, even though this biomaterial was opaque.

Although I did not used soluble elastin in experiments in this thesis, future work may require it. The accepted method for solubilizing elastin for solubilized elastin was as follows. To break elastin down to a size soluble in water (12,000–20,000 molecular weight), elastin was solubilized by heating in a 1M KOH 80% ethanol solution. This solution was stirred for 2.5 hours at 50°C. As the elastin dissolved, the solution turned a clear yellow. Next 10 ml deionized water was added, and the solution was titrated with concentrated HCl to a pH of 7. After cooling to 4°C overnight, the solution was centrifuged for 15 minutes at 2000 rpm. The supernatant was transferred to dialysis tubing and dialyzed against tap water until the dialysis water's absorption spectrum matched the tap water's absorption spectrum over 200-800 μm. Then the solution was dialyzed against deionized water. Finally, the solution was dry frozen into powder. This process required approximately four days. The yield was 61%.

Originally, cryoprecipitates that contained fibrinogen, fibronectin, and factor XIII were generated from pooled pig blood. However, the synthesized cryoprecipitates produced good biomaterial inconsistently. Using fibrinogen ordered from Sigma produced good biomaterial consistently, even though fibrinogen does not contain fibronectin and factor VIII that have been shown to increase biomaterial strength [22]. However, fibrinogen–only–based–material is adequately strong for studying welding. In the future, others will need to generate cryoprecipitates. The standard

method is as follows. Fresh blood was transferred to 50 ml centrifuge tubes and spun at 1500 rpm for 15 minutes. The plasma was collected and stored at −70°C overnight, and then was thawed slowly at 4°C. Next, the plasma was centrifuged at 1500 rpm for 15 minutes. The supernatant was decanted off, leaving approximately 3 ml of precipitate in each tube. Then 2 ml of 0.9% NaCl, 0.66% $C_6H_5Na_3O_7$ was added to each 50 ml tube, and the result was dry frozen. This process took three days, not including dry freezing time. 700 ml of plasma yielded 5.8 g of precipitate.

2.2 Steady–State Thermal Experiments

To elucidate the thermal factors involved in welding, several experiments were conducted on the biomaterial at steady–state temperatures in a water bath. A hot water bath consisting of a large beaker of water was heated to the desired temperature by a hot plate. The temperature was monitored with a thermometer. A stirring bar kept the temperature uniform (Figure 2.2.1). Later experiments used a commercial waterbath (Equatherm), that maintained constant temperatures to within a degree. The temperature was monitored by a thermometer or thermistor.

2.2.1 Thermal Tests

The first experiments were made on pieces of biomaterial brought to room temperature in 0.9% saline solution after being stored in 33% ethanol. Samples were cut into approximately 1 cm^2 pieces. The pieces were immersed using a pair of tweezers. Observations were made at various temperatures between 50–100°C for two minute immersions. At higher temperatures vegetable oil was used instead of water. Observations were made between 90–130°C.

2.2.2 Biomaterial to Porcine Aorta Welds

Preliminary attempts were made to weld biomaterial to porcine aorta. According to our thermal tests, the only noticeable change in the biomaterial occurred above 64°C, indicating a possible denaturing or melting point. Consequently, welds were attempted at 60 and 70°C in an Equatherm water bath. Because others have achieved strong welds with pressure, a steel plate weighing 1 kg was wrapped in aluminum foil to protect the samples from rough edges of the plate [13]. The aorta was placed intimal side up on the foil, and then the biomaterial was placed on top. The block and samples were carefully wrapped in another piece of foil so that there was good contact maintained between aorta and biomaterial while being transferred to and from the bath (Figure 2.2). Welds were attempted at 60 and 70°C for 5 minutes each using the steel block.

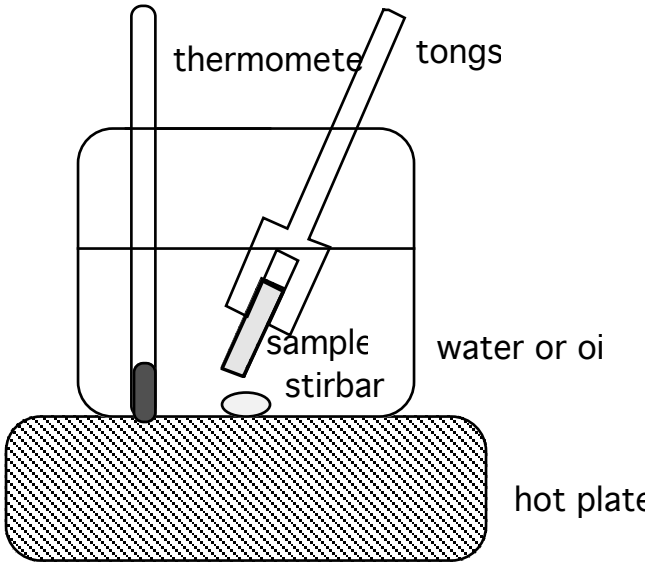

Figure 2.1: Thermal tests of elastin-based biomaterial in a heated beaker.

Another weld was attempted at room temperature outside the water bath for five minutes. Welds were attempted at various temperature in the range of 60–80°C for 2 minute immersions.

To verify that foil maintained good contact between aorta and biomaterial during immersion, welds without foil were attempted at 75°C for 10 minute immersion. Yet another method of contact was tested by clamping biomaterial and aorta between steel washers with binder clips at 79°C and at room temperature for 10 minutes (Figure 2.3).

2.3 Penetration Depth of Indocyanine Green

Indocyanine Green (ICG) is the most widely used colorimetric indicator for circulatory studies [28]. It has a peak absorption at 805 nm when bound to albumin, and a peak at 774 nm when dissolved in water (Figure 2.4). ICG degrades over time when exposed to light, so proper storage in a light–tight environment is important for ensuring the same ICG quality with each staining [28]. ICG was the absorbing chromophore in all our experiments. I measured the penetration depth of ICG dissolved in water, albumin and healon glue on both fresh and thawed aorta. A saturated solution of 5 mg/ml of ICG was used. After the ICG solution was applied with a disposable pipette the ICG was allowed to soak into the aorta for 1, 2, 3, 4, 5, 10, 15, and 20 minutes before being blotted away using cheese cloth. The samples were frozen for easier observation under the microscope. Cross sections of aorta were made, and the depth of penetration

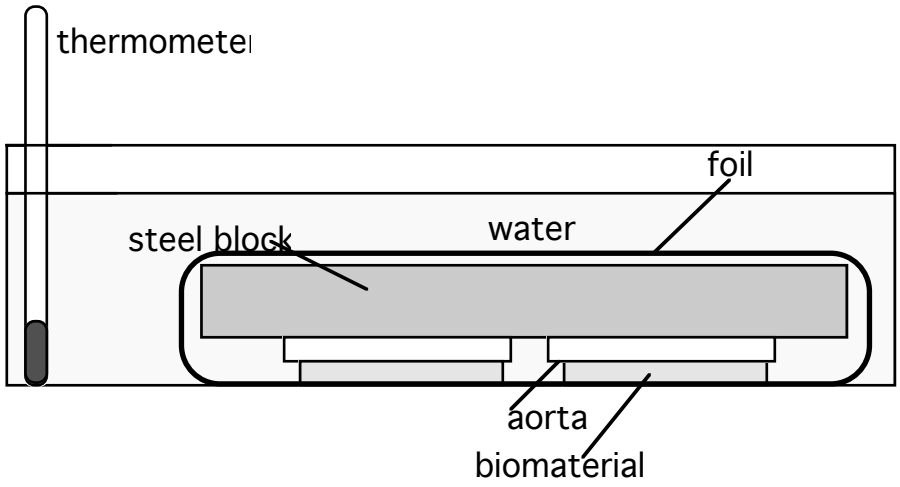

Figure 2.2: Waterbath welds between biomaterial and porcine aorta in an Equatherm waterbath under pressure

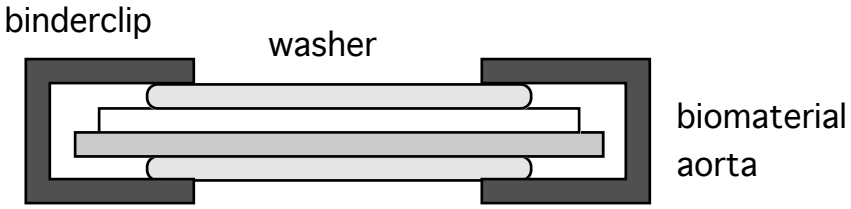

Figure 2.3: Waterbath welds with samples held between washers in an Equatherm waterbath.

was measured using a reticule in the eyepiece.

.

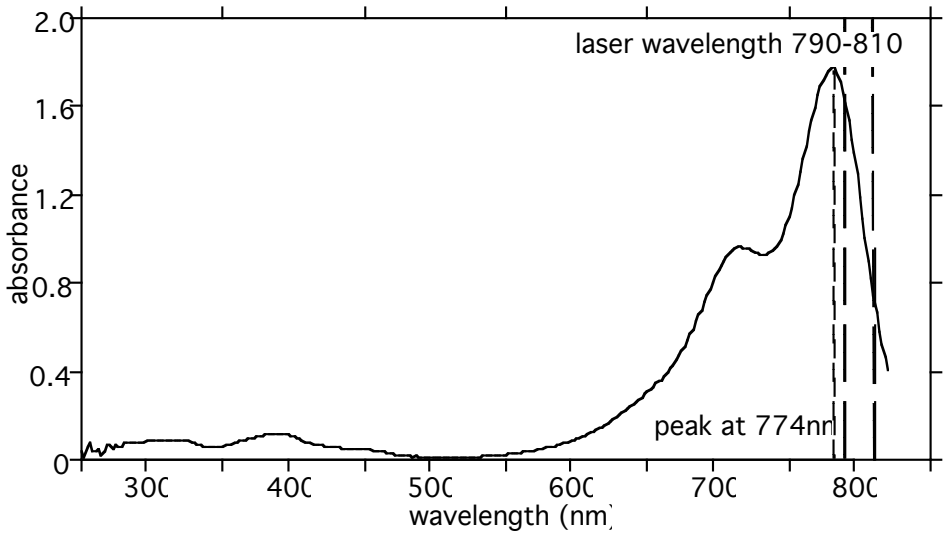

Figure 2.4: Absorption spectra of Indocyanine Green (ICG) in water.

2.4 ICG Transmission Measurements

ICG bleaches from green to orange after exposure to a series of diode laser light pulses. Bleaching of ICG was assessed on thawed aorta that was immediately stained with 5 mg/ml ICG dissolved in water. The intima of thawed aorta was stained with ICG solution by using a disposable pipette to spread the ICG evenly. Any excess solution was blotted away using cheesecloth. The aorta was kept under cheesecloth moistened with saline to prevent dehydration. Pieces of aorta were trimmed to approximately 2×3 cm to fit between two glass slides, and the slides were held together using tape.

The laser source was a pulsed diode laser operating at wavelengths between 790–810 nm (Star Medical Technologies). Either a 3×3 mm or a 6×6 mm in size condenser was fitted on the handpiece of the laser, yielding a uniform square spot. The condenser was placed flush against the glass slide when the laser was fired. The stained side of the aorta was situated closest to the condenser. Pulse durations of 0.5–5 ms and pulse energies of 0.15–3.25 J could be independently selected.

Optimum power was maintained by keeping the condenser in good condition. The inside

of the condenser was made from copper sheeting and was easily tarnished by excessive heat, resulting in a decrease in pulse energy. Whenever the pulse energy dropped, Brass-O was used to polish the inside of the condenser, restoring the surface to maximal reflection.

An integrating sphere six inches in diameter coated with 98% reflecting Spectralon (Labsphere) was used to make transmission measurements of the stained aorta. The sphere had four ports evenly spaced around the equator of the sphere. The sample of stained aorta was placed in front of a port so that the sample completely covered the port hole. The diode laser handpiece was mounted so that the condenser was flush against the sample. A silicon photodiode detector was mounted 90° from the sample. The other two ports were plugged. An internal baffle between the entrance port and the detector port prevented light from the sample from reaching the detector before being diffusely scattered (Figure 2.5).

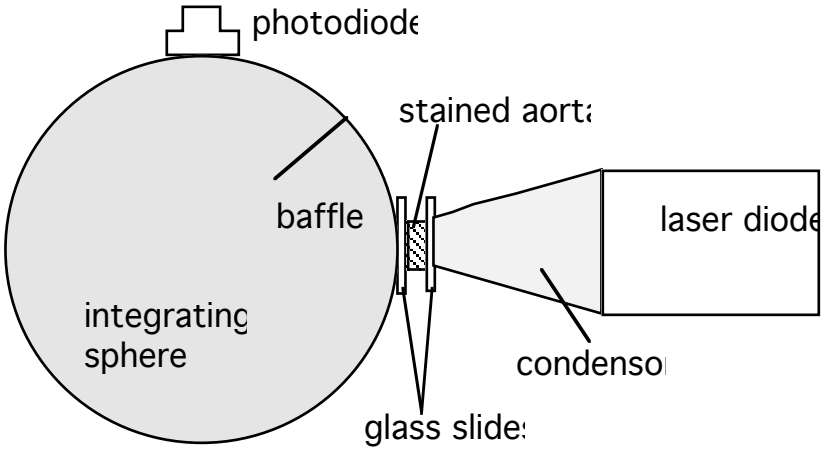

Figure 2.5: Transmission measurements set-up.

The pulse length was held constant and the pulse energy was varied to test bleaching over a range of radiant exposures. The laser was set to deliver 0.5, 1, 3, and 5 ms pulses. Transmission measurements were done using the 6×6 mm and 3×3 mm condensers. (Table 2.1). A change in voltage reading was taken after each pulse. Transmission measurement of an unstained piece of aorta was used as a reference for maximum transmission. Transmission was calculated as the ratio of the voltage change for stained aorta to the voltage change for unstained aorta.

Table 2.1: Laser parameters used in bleaching experiments.

Pulse Duration (ms)	3×3 mm condenser Radiant Exposure (mJ/mm^2)	6×6 mm condenser Radiant Exposure (mJ/mm^2)
0.5	13	6
0.5	20	9
0.5	22	10
1	26	13
1	33	17
1	36	19
1		20
3	18	16
3	38	22
3	56	26
3	84	37
3	94	48
3		55
5	31	16
5	66	28
5	93	37
5	129	54
5		66
5		92

2.5 Thermal Measurements

Thermal measurements of ICG stained aorta during laser irradiation are essential to assess the relationship between temperature and welding. Temperatures were measured using a HgCdTe detector (EG&G Judson) with a range of 8–12 μm. The size of the detector was 1×1 mm. The detector had a 60 degree field-of-view provided by a cold stop to minimize background radiation. The detector was cooled with liquid nitrogen. A cold filter with a 90% transmission between 8–11.5 μm was also included[¶]. The system was mounted to a side-view metal dewar with an eight hour liquid nitrogen holding time. On the front of the cold filter, a detector window 0.40 inches thick was mounted. The detector window made of ZeSe had a greater than 74% transmission between 500 nm and 20 μm. Directly behind the finger, the cold filter was mounted. The detector was centered and mounted (Figure 2.6). The detector required half an hour to cool after the dewar was filled with liquid nitrogen. The liquid nitrogen supply must be replenished every two hours.

A preamplifier designed for AC/DC operation with a bandwidth of 1.5 MHz was chosen. Low noise ($\leq$5 mV) $\pm$15 V power supply was required for use with the preamplifier. The preamplifier and detector were impedance-matched to each other.

The detector has a 60 degree field-of-view, so the optical system was designed to collect as much light as possible and fill the detector uniformly over 60 degrees. Germanium lenses were chosen because the index of refraction of germanium is 4.0 throughout the wavelength range of 8–12 μm, eliminating chromatic aberration.

I decided to use two lenses to image a one-to-one spot from sample to detector. Space was required for any apertures mounted in front of the optical system and for the positioning of the laser source. The shorter the focal length of the individual lens and the larger the diameter of the lens, the greater the field of view. I compromised by limiting the diameter of the lenses to an inch and the focal length to 50 mm.

A ray tracing program, `Beam 3`, was used to compare various lenses and lens systems. The detector must be able to collect light from all areas of the sample, but not beyond the sample edges. After several simulations to test spherical aberrations two 1.0 inch diameter plano-convex lenses with 50 mm effective focal lengths were chosen. These lenses resulted in a 28 degree field-of-view. The distance between lenses did not significantly affect spherical aberrations or the

[¶]This particular filter was chosen since observations of wavelengths highly absorbing for water were of interest because tissue is mostly composed of water.

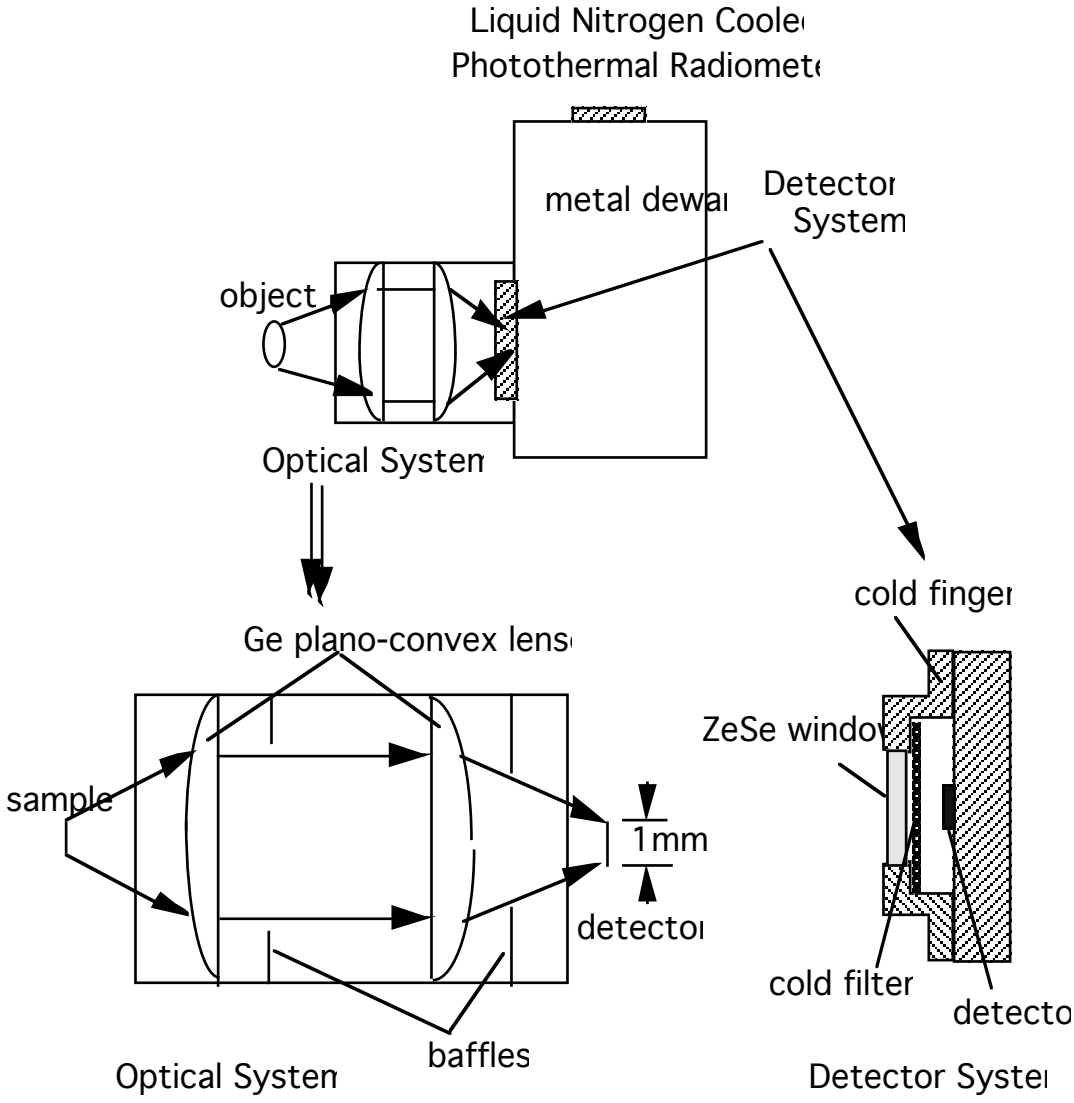

Figure 2.6: The photothermal radiometer (not drawn to scale). The detector was a HgCdTe detector, sensitive 8–12 μm. The optical system was designed to image a 1 mm spot from the sample to the 1 mm spot of the detector.

field-of-view, even though theoretically the optimal distance between lenses is 2 effective focal lengths. Meniscus lenses showed no advantage over plano-convex lenses in reducing spherical aberrations, and were more expensive.

The optical housing is a threaded aluminum tube. The tube was secured to the dewar with three set screws. The threads served two purposes. Brass lens holders, 0.25 inches thick and two inches in diameter with an inner diameter of 1 inch with a 0.94 inch lip to hold the lens, were threaded around the outer diameter to match the threads on the aluminum tube. The second purpose of the threads was to reduce stray light by acting as a diffusing surface.

To ensure that stray light did not reach the detector, I evaluated baffles using `Beam 3`. 1/2 inch and 1/4 inch baffles were chosen. The baffles were made out of brass and threaded along the outside diameter, similar to the brass lens holders. The 1/2 inch baffle was placed between the two lenses, and the 1/4 inch baffle was placed in front of the detector system.

To align the system the 1/4 inch baffle is screwed as far down the tube as possible. The position of the first lens was found by using a heat source placed 3 m away. The position was determined by the maximum signal as the lens was moved along the tube. Next, the 1/2 inch baffle was placed in the tube. Then, the second lens was located near the outer edge of the tube to maximize the focal length outside the tube.

2.5.1 Calibration of the Photothermal Radiometer

The photothermal radiometer was calibrated using two aluminum blocks (one inch cubes) painted with black spray paint on one face (Figure 2.7). Each face had centered holes an eighth of an inch in diameter for placement of a thermistor to monitor the temperature. The hole on the spray painted face also served as a black body emitter. One block was heated on a hot plate and the other was kept in an ice bath at 1°C. At temperatures ranging from 22–100°C, the heated block was placed at the focal point of the photothermal radiometer, and then quickly replaced by the cooled block. The peak-to-peak voltage change between the heated block and the cooled block was taken for several temperatures of the heated block. The slope of a linear curve fit of this data yielded the voltage change per degree Celsius. Two calibrations were made, with and without a 5 mm diameter aperture placed 5 mm away from the edge of the optical tube of the photothermal radiometer.

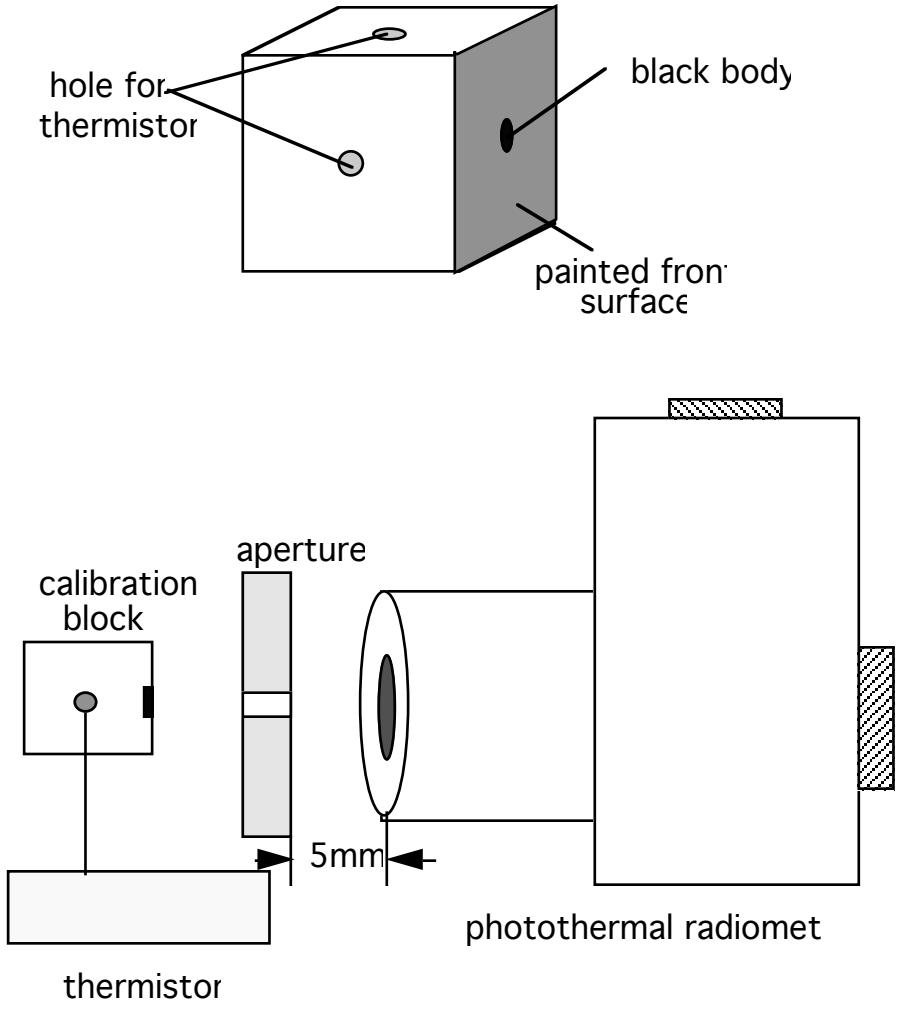

Figure 2.7: Calibration block and set-up for the photothermal radiometer.

2.5.2 Thermal Measurements of Bleaching Stained Aorta

Thermal tests were done on stained aorta that had been stained with 5 mg/ml ICG in water and massaged into the aorta. The sample, approximately 2×3 cm in area, was placed at 45 degrees to both the photothermal radiometer and the diode laser (Figure 2.8). The laser was positioned 90 degrees from the photothermal radiometer and as close to the sample as possible without blocking the view of the photothermal radiometer. A fresh site of aorta was used for each pulse energy tried. Several areas of the sample were used for each measurement. The radiant exposures delivered by the laser with the 3×3 mm condenser are given in Table 2.2. Also included are single pulse measurements completed during the following simultaneous transmission and thermal experiment, which is described in the next section. In that experiment, the first pulse measurements using the 3×3 mm condenser were repeated only at 5 ms pulse duration, and new measurements using the 6×6 mm condenser were done, also at 5 ms pulse duration.

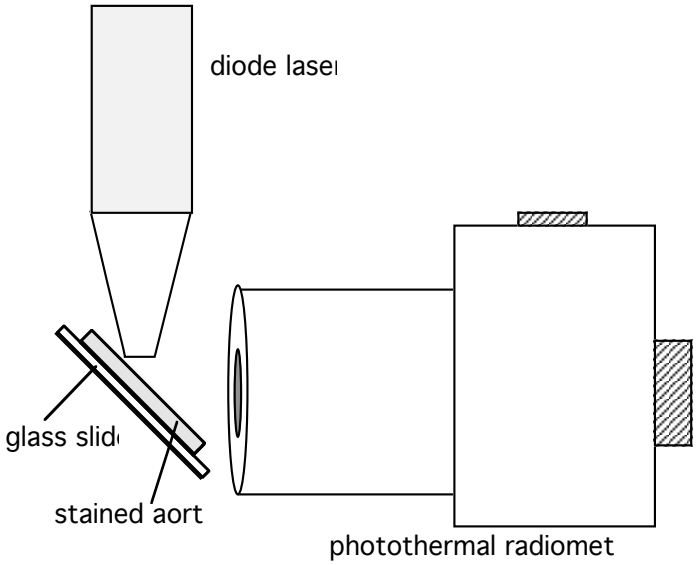

Figure 2.8: Apparatus for thermal measurements. Sample is at 45 degrees to both the laser and the photothermal radiometer.

2.6 Simultaneous Transmission and Thermal Measurements

To confirm the trends found in separate transmission and thermal measurements, simultaneous bleaching and thermal measurements were made using the experimental arrangement shown in

Table 2.2: Parameters for single pulse thermal measurements using 3×3 mm and 6×6 mm condensers.

Pulse Duration (ms)	Radiant Exposure 3×3 mm (mJ/mm^2)	Radiant Exposure 6×6 mm (mJ/mm^2)
1	27	
3	63	
3	74	
5	38	42
5	52	51
5	63	59
5	74	68
5	83	76
5	100	86
5	110	
5	122	

Figure 2.9.

The pulsed diode laser was placed at 90° to the photothermal radiometer by aligning with a HeNe laser (not shown). A glass slide was placed at the focal point of the optical system of the photothermal radiometer and rotated 45 degrees. The HeNe beam was then split at 90 degrees. The laser was placed so that the HeNe beam was inside the condenser. The sample of freshly stained, previously frozen aorta was placed at the focal point of the photothermal radiometer 45° to both photothermal radiometer and laser. The laser was moved as close to the sample as possible without blocking the detector. The integrating sphere was positioned directly behind the sample for transmission measurements. The only difference from the transmission-only experiment was that the top glass slide was removed and the laser light was incident at 45 degrees on the sample. The oscilloscope was triggered by diffuse laser light reaching the detector. Measurements were taken between 38–122 mJ/mm^2 and 42–88 mJ/mm^2 using the 3×3 mm and 6×6 mm condensers respectively.

Transmission and thermal measurements were taken for at least ten successive pulses at one spot site. The sample was allowed to cool for at least 30 seconds between pulses to evaluate heating by each pulse. Subsequently 4–8 first pulse thermal measurements were made by moving to new places of the sample for each pulse. (Table 2.2).

Another set of measurements was done using the 4×4 mm condenser, 5 ms pulse duration,

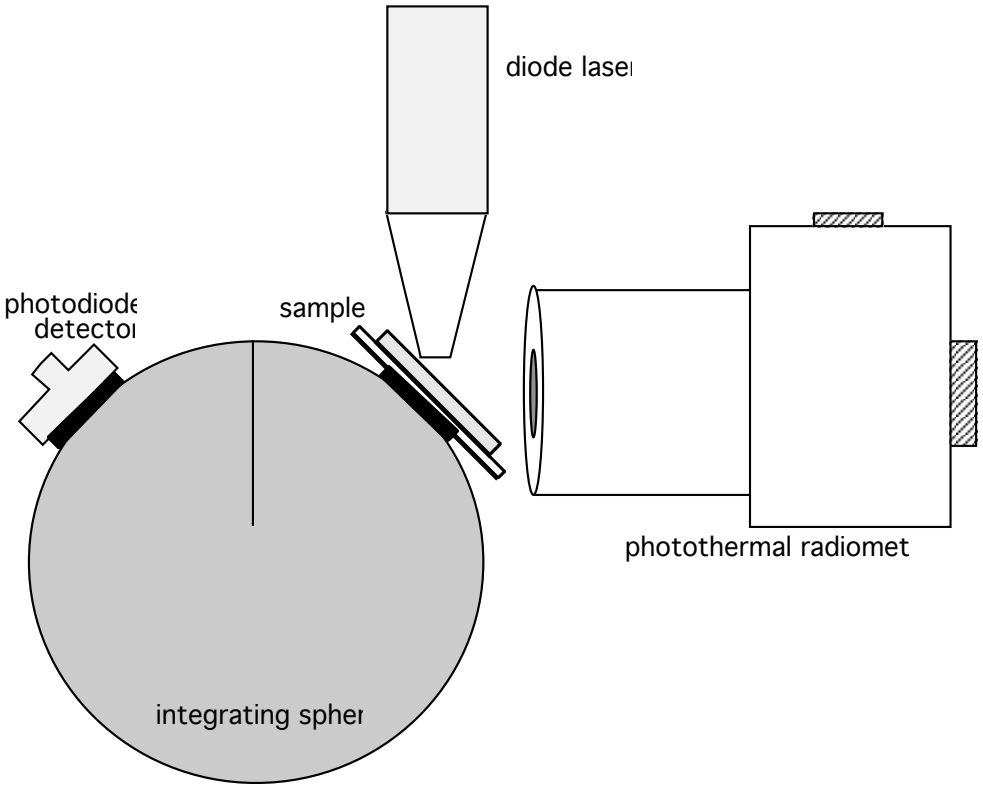

Figure 2.9: Apparatus for simultaneous transmission and thermal measurements.

and 9.7 mJ/mm^2 radiant exposure. These measurements were repeated ten times.

2.7 Welding

Two methods of welding were tried. First, welds without significant pressure added to the sample were attempted. The only pressure present was pressure applied by holding the sample together with masking tape. In the second method exerted pressure by pressing firmly down on the sample with a brass ring that uniformly distributed the force over the area of the sample.

2.7.1 Welding without Pressure

A stained piece of aorta approximately 2×3 cm was mounted on a glass slide. A slightly smaller piece of biomaterial was placed on top of the aorta, and another glass slide rested on top. The biomaterial sandwich was then taped together using masking tape. At three spots on the sample, with the laser set at 76 mJ/mm^2, 5 ms pulse length, 6×6 mm condenser, the laser was fired 10 times as fast as possible (approximately 2 Hz), 20 times at 1 Hz and 10 times at 0.5Hz. Another attempt was made using the 3×3 mm condenser at 74 mJ/mm^2, 3 ms pulse length, fired at 1, 3, 5, and 10 pulses.

Another experiment used the 6×6 mm condenser at 76 mJ/mm^2, but the biomaterial was stained with ICG on both sides. Seven pulses at 2 Hz, 7 pulses at 0.5 Hz and 20 pulses at 2 Hz were made at three separate places on the sample.

Laser welds without pressure used biomaterial stained only on one side. 10, 15, and 20 pulses were fired at 2 Hz. Another attempt was made using the 3×3 mm condenser at 3 ms pulse length, 74 mJ/mm^2 at 1, 3, 5, 7, and 10 pulses.

2.7.2 Welding with Pressure

To determine the pressure needed to make a strong weld of biomaterial to aorta a glass slide, biomaterial, aorta, slide sandwich was used as the sample. A scale that measured up to 2.5 kg, and a brass ring to exert the pressure completed our apparatus (Figure 2.10). The condenser fit within the ring. The sample size of the aorta/biomaterial sample varied from 1 cm^2 to 1.5 cm^2. (Table 2.3).

To determine how water in and on the sample affected the pressure needed for welding, the biomaterial was blotted on a paper towel, and then welded without pressure, yielding a medium strength weld.

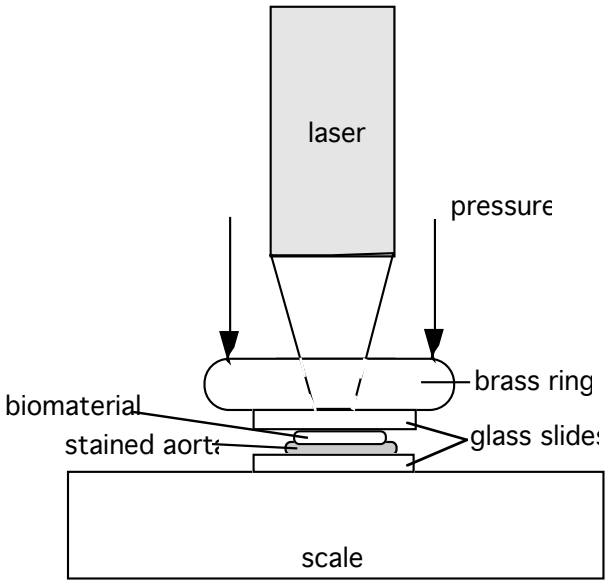

Figure 2.10: Welding with pressure monitored by a scale. Pressure is applied to the brass ring. Radiant exposure was 86 mJ/mm^2 using the 3×3 mm condenser and 5 ms pulse duration.

Table 2.3: Parameters for welding with pressure using 86 mJ/mm^2 radiant exposure and 5 ms pulse duration.

Weight (kg)	Area (cm^2)	Pressure (N/cm^2)
1.0	1.95	5.0
1.2	1.32	8.9
1.2	1.87	6.3
1.5	3.06	4.8
2.0	1.00	19.6
2.0	1.32	14.8
2.0	1.56	12.6
2.0	1.68	11.7
2.0	1.69	11.6

Chapter 3

Results

The Results Chapter directly parallels the Methods Chapter.

3.1 Biomaterial

All experiments used biomaterial made with fibrinogen and without fibronectin and factorXIII. The biomaterial was consistently elastic, opaque and strong. It had properties similar to tissue in that it was mostly composed of water and was nearly transparent at 808 nm light.

3.2 Steady-State Thermal Experiments

The biomaterial retained its shape and strength during all thermal tests below 100°C. The welds were generally successful as long as sufficient contact was maintained during welding. In some cases, welds were so strong that the biomaterial ripped before the weld failed. Typically 70°C with 5N/cm^2 of pressure were required for 5 minutes to achieve strong welds.

3.2.1 Thermal Tests

Initial thermal tests were made to determine the basic properties of the biomaterial as it underwent heating. Unheated biomaterial is opaque and has the consistency of a wet noodle except that it is stronger and more elastic. At 53 and 60°C no change was noted in the material after 1.5 minutes. For temperatures between 64 and 92°C the only noticeable change was air bubbles forming on the surface of the material. In every case the biomaterial did not lose its shape or thickness, and appeared to have the same strength. For pieces submerged in oil, no change was noted in the biomaterial at 90 and 95°C. At 104°C after one minute the biomaterial had a

deep-fried appearance and had lost its elasticity. At 130°C after one minute the biomaterial was completely deep-fried. The best description of its appearance is a fried pork rind.

3.2.2 Biomaterial to Porcine Aorta Welds

The initial welding experiment was done in a water bath to determine how much heat was required to achieve a weld. Results are shown in Table 3.1 below.

Table 3.1: Biomaterial to porcine aorta welds under pressure. Welds were successful between 65–80°C when pressure was applied.

Temperature (°C)	Time (min)	Weld Strength
27	5	*none*
62	5	*weak weld at edges only*
64	5	*none*
67	5	*none*
72	5	*weak weld at edges only*
77	5	*weak weld at edges only*
82	5	*none*
75	5	*very good (washers used)*
79	5	*very good (washers used)*

Both samples of biomaterial after immersion for five minutes in a 70°C water bath appeared flattened, and bubbles were apparent. The welds could be pulled apart using tweezers. The resistance of the weld to being pulled apart was comparable to pulling a bandaid off skin. At some places the weld was stronger than the biomaterial.

No welds were achieved at 60°C and at room temperature after five minutes. The biomaterial was easily lifted off the aorta. No air bubbles were observed, but the biomaterial had been flattened.

No welds were achieved for samples in the water bath for two minutes between 62–82°C. The only incidence of welding was at the edges and at the corners of the biomaterial, but not at the center.

Welds were achieved at 79°C for welds sandwiched between washers. The welds were very strong—the biomaterial ripped before the weld came apart. At 75°C an extremely strong weld was made when the sample was submerged directly beneath the steel block, without being wrapped

in foil. The biomaterial was flattened, but still maintained its strength and elasticity. There were no welds at room temperatures.

3.3 Penetration Depth of Indocyanine Green

ICG dissolved in either albumin or healon glue did not penetrate well or evenly into the aorta. The stained aorta appeared grainy with approximately 100 μm diameter spots. ICG dissolved in water penetrated the intimal side of aorta to depths varying between 100-400 μm. The depth was difficult to measure because the ICG seemed to soak through in layers—the inner layers were lighter or less concentrated than the outer layers. Because ICG in water penetrated about 200 μm for most samples independent of time soaked, 200 μm was used as the penetration depth and the optical zone in all our calculations.

Direct staining of aorta varied with technique. A dark stain was achieved when ICG was dropped onto the aorta and allowed to soak. A lighter less uniform stain was achieved when ICG was dropped on and then massaged into the aorta.

3.4 ICG Transmission Measurements

Transmission measurements on ICG-stained aorta were conducted using a single integrating sphere apparatus and photodiode (Figure 2.5). Figure 3.1 shows the transmission during a pulse. The transmission increased with each pulse. This was typical of samples in which a visible color change from green to orange occurred.

Transmission measurements of unstained aorta were made as a reference for total transmission. Transmission was calculated from voltage data of stained tissue divided by voltage data of unstained tissue:

$$T = V/V_u$$

where V is the voltage for stained tissue, and V_u is the voltage for stained tissue.
In the following figures, transmission was calculated at various radiant exposures for several pulse durations. At higher radiant exposures note the increase in transmission to a maximum value of about 80%.

Figure 3.2 shows transmission over several pulses at 0.5 ms pulse duration and 1 ms pulse duration for various radiant exposures using the 3×3 mm condenser. Notice that the increase

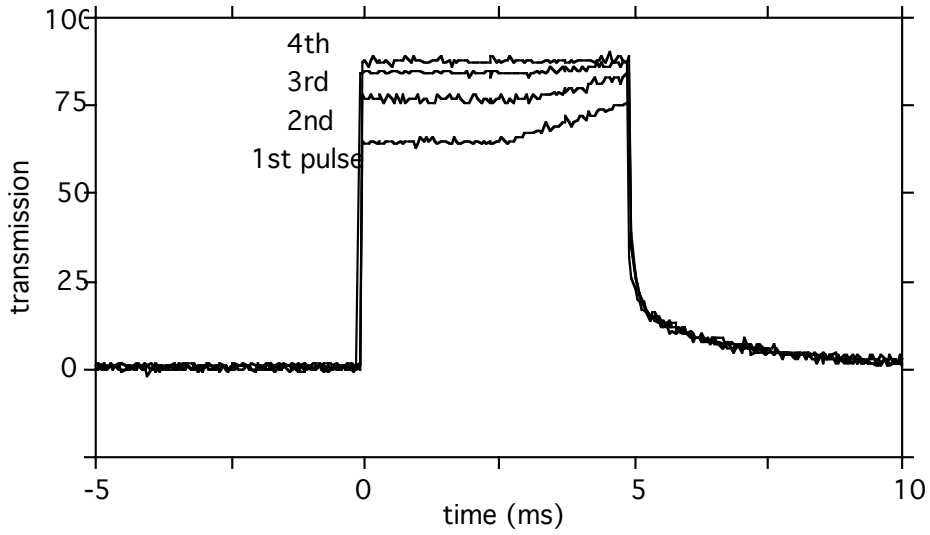

Figure 3.1: Increase in transmission over several pulses using the 3×3 mm condenser at 1.1 J per pulse that lasts for 5 ms.

in transmission is more apparent for the 1 ms pulse than for the 0.5 ms pulse. At longer pulse durations of 3 ms and 5 ms with higher radiant exposures, the increase in transmission is present (Figure 3.3). The 6×6 mm condenser yields smaller radiant exposures, and the increase in transmission is not as large as for the smaller condenser (Figure 3.4). However, at longer pulse durations, some increase is still noted (Figure 3.5).

The bleaching effect observed consisted of a faint pale spot that deepened into an orange square spot the size of the condenser with more pulses. The first appearance of pale orange was defined as faint bleaching. At sufficient radiant exposure, the orange bleaching appeared shiny with each successive pulse. This visual change in appearance was defined as maximum bleaching in the following tables. Further laser pulses darkened the orange spot, and the spot spread approximately 1 mm beyond condenser dimensions. This effect was noted only at the highest radiant exposure for each condenser.

Speckling of the ICG was noted in some cases before visible bleaching was observed. See Table 3.2 and Table 3.3. Speckling appeared to be a concentration of ICG in the area of the laser spot where before laser exposure, the stain was uniformly green.

For energies where no bleaching was noted, the transmission stays nearly constant. Steady increases in transmission corresponded to an observation of bleaching, especially in cases where shininess was noted. This trend was more apparent for data taken with the smaller condenser.

At the highest pulse energies a large increase in transmission with successive pulses did not occur because of no bleaching, but because maximum bleaching occurred in the first or second pulse.

Table 3.2: Bleaching observations using the 3×3 mm condenser. Bleaching corresponded to an increase in transmission over several pulses. At higher radiant exposures, maximum bleaching occured within a few pulses.

Pulse Duration (ms)	Radiant Exposure (mJ/mm^2)	Faint Bleaching (pulses)	Maximum Bleaching (pulses)	Comment
0.5	13			*No bleaching*
0.5	20			*Speckling*
0.5	22			*No bleaching*
1	26	2	10	
1	33	2	5	
1	36	2	8	
3	18			*No bleaching*
3	38	3	10	
3	56	1	3	
3	84	1	3	
3	94	1	4	
5	31			*No bleaching*
5	66	1	5	
5	79		1	
5	93		1	
5	129		1	*Larger bleached area*

Table 3.3: Bleaching observations using the 6×6 mm condenser. Bleaching corresponded to an increase in transmission over several pulses. At higher radiant exposures, maximum bleaching occured within a few pulses.

Pulse Duration (ms)	Radiant Exposure (mJ/mm^2)	Faint Bleaching (pulses)	Maximum Bleaching (pulses)	Comment
0.5	6			*No bleaching*
0.5	9			*No bleaching*
0.5	10			*No bleaching*
1	13			*Speckling*
1	17	2		
1	19	2		
1	20	2		
3	16			*No bleaching*
3	22	10		*Speckling*
3	26	5	13	
3	37	1	7	
3	48	1	7	
3	55	1	3	
5	17			*No bleaching*
5	28	4		
5	37	2	10	
5	54	1	7	
5	66	1	2	
5	91		1	*Larger bleached area*

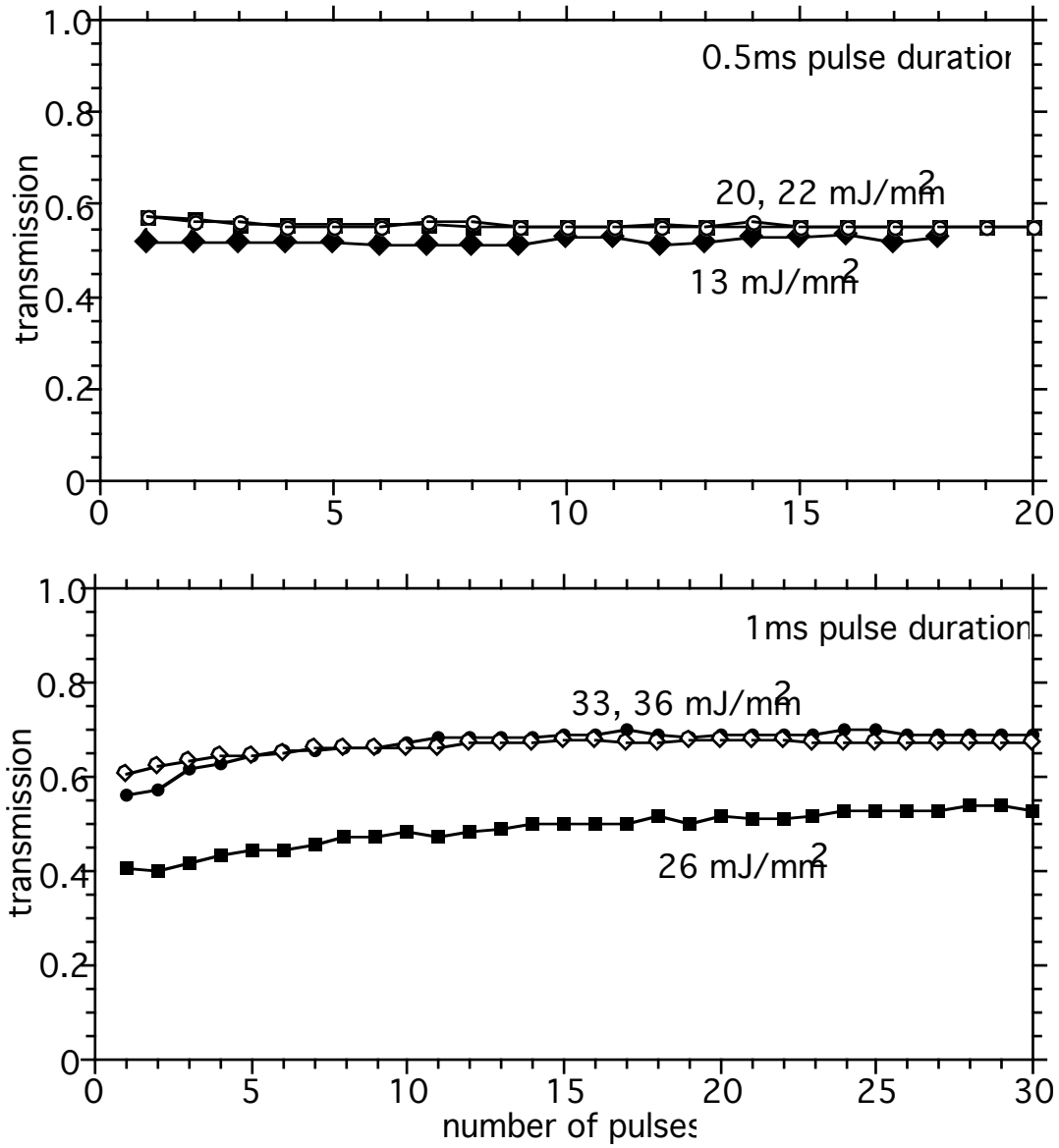

Figure 3.2: Transmission for 0.5 ms and 1 ms pulse durations, 3×3 mm condenser. Radiant exposure was not high enough to cause bleaching.

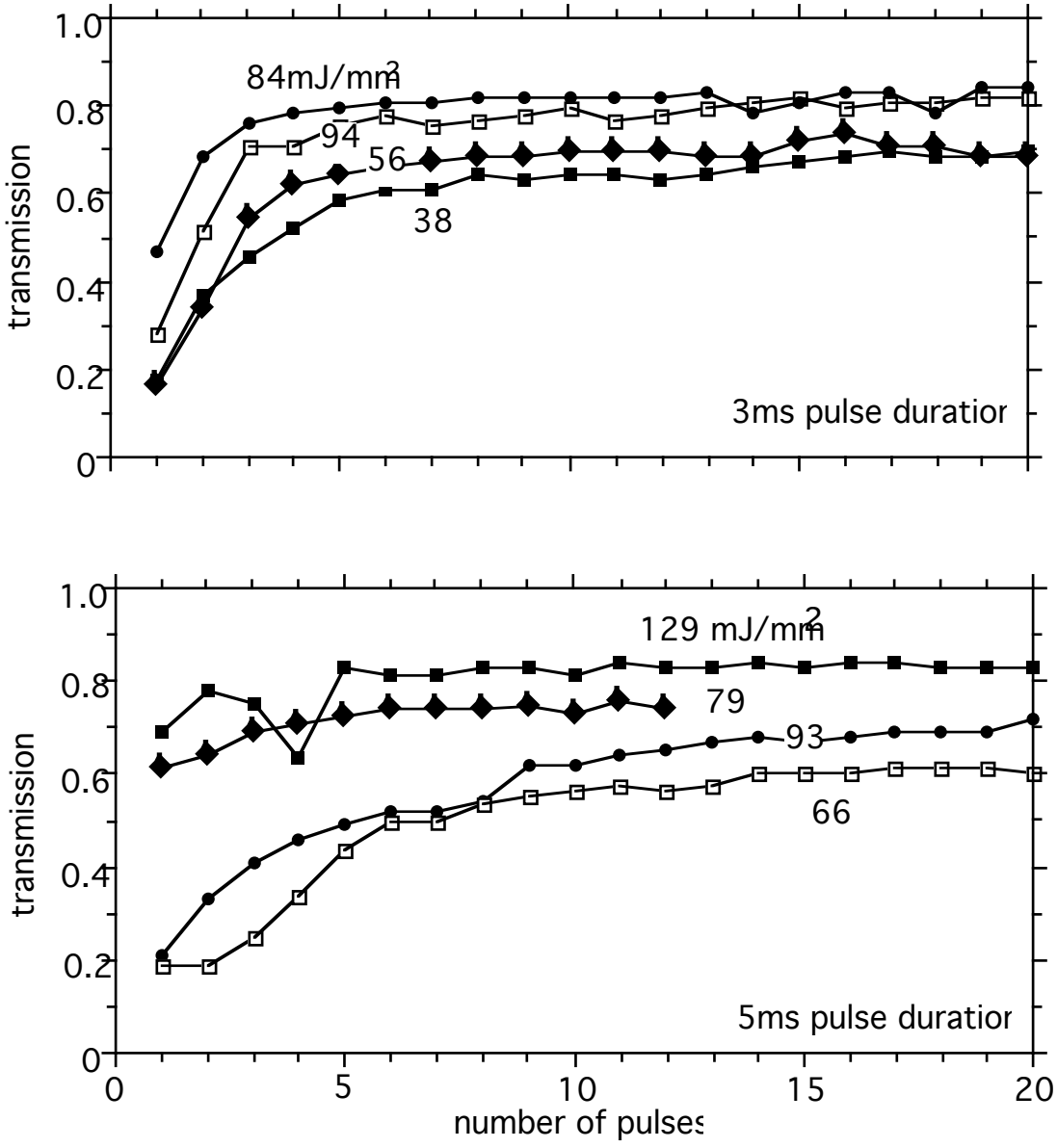

Figure 3.3: Transmission for 3 ms and 5 ms pulse durations, 3×3 mm condenser. At these radiant exposures bleaching occurred over 1-5 pulses before reaching a maximum.

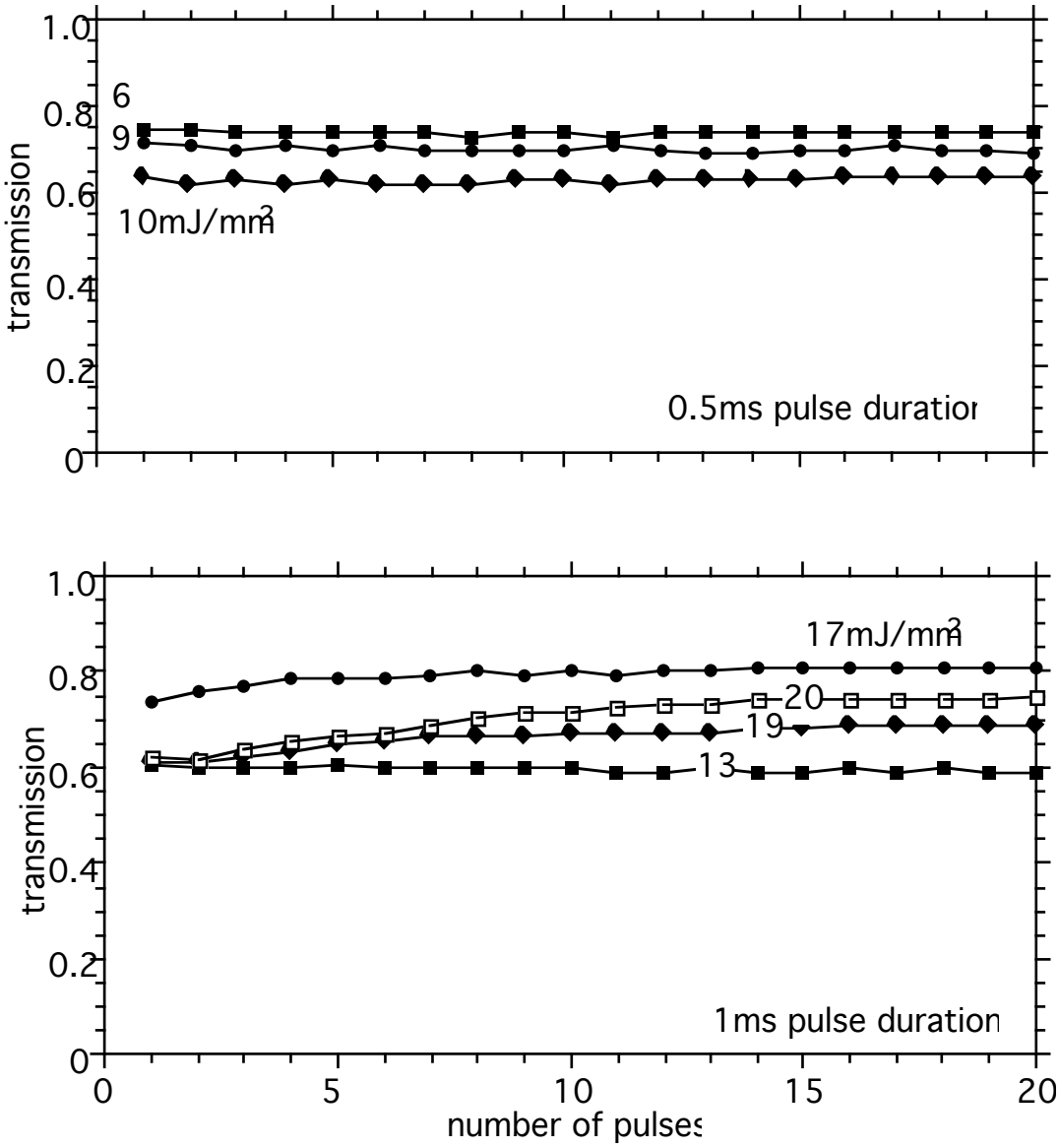

Figure 3.4: Transmission for 0.5 ms and 1 ms pulse durations, 6×6 mm condenser. Radiant exposure was not high enough to cause bleaching.

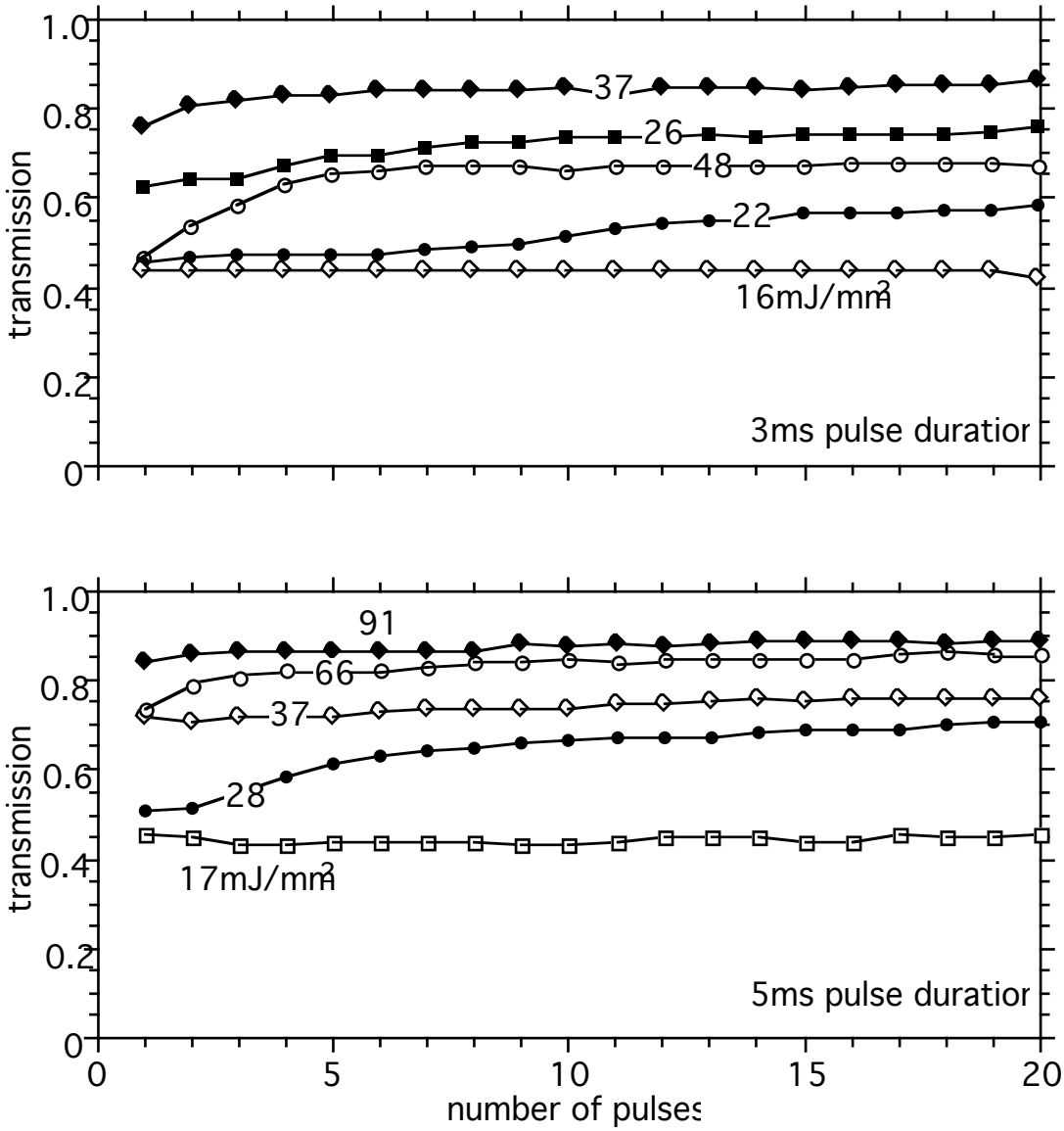

Figure 3.5: Transmission for 3 ms and 5 ms pulse durations, 6×6 mm condenser. For higher radiant exposures, bleaching occurred within a few pulses, corresponding to an increase in transmission over those pulses.

3.5 Thermal Measurements

3.5.1 Calibration of the Photothermal Radiometer

For the calibration done without an aperture, the detector saturated at temperature changes above 50°C (Figure 3.6). This maximum temperature change was insufficient for most measurements with heated tissue. Another calibration was done with an aperture 0.5 cm in diameter placed 5 mm away from the lens system. The detector saturated at a 140°C temperature changes with this aperture (Figure 3.7). This aperture was used for all measurements.

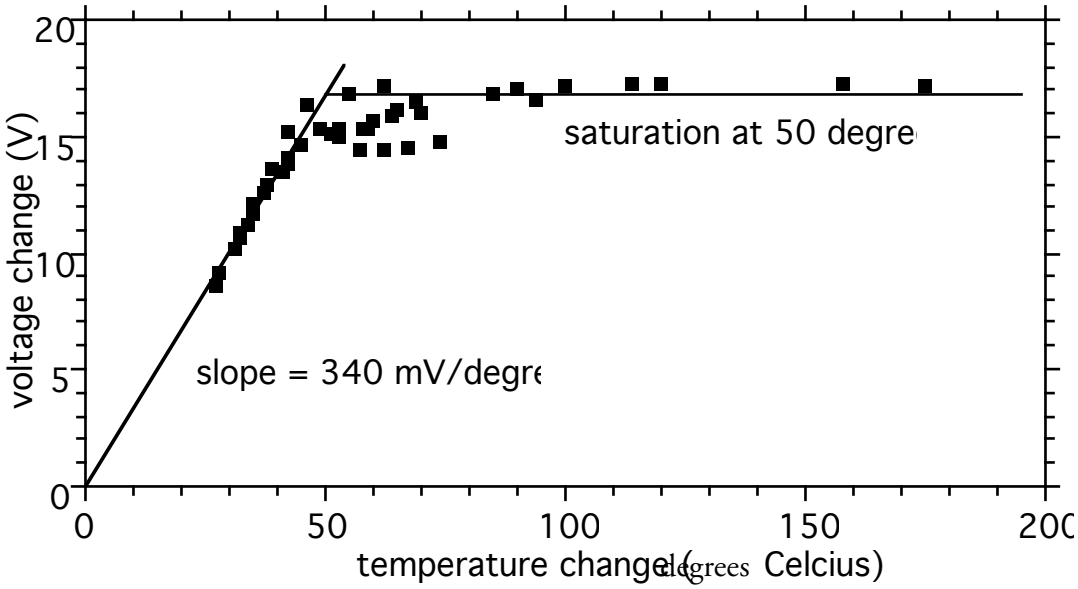

Figure 3.6: Calibration curve of photothermal radiometer without aperture. Saturation occurred at 50°C which was too low for most measurements of heated tissue for welding.

3.5.2 Thermal Measurement of Bleaching Stained Aorta

A typical thermal response for irradiated stained aorta is shown in Figure 3.8.

A linear increase in temperature was observed over radiant exposure. Error bars represented the standard deviation of several first pulse measurements of the same stained aorta. Three different pulse durations were used. Since the points fall within the line suggesting for all pulse durations, that indicates that temperature depends on radiant exposure and not on power.

$$T = \frac{\mu_a E}{\rho c}$$

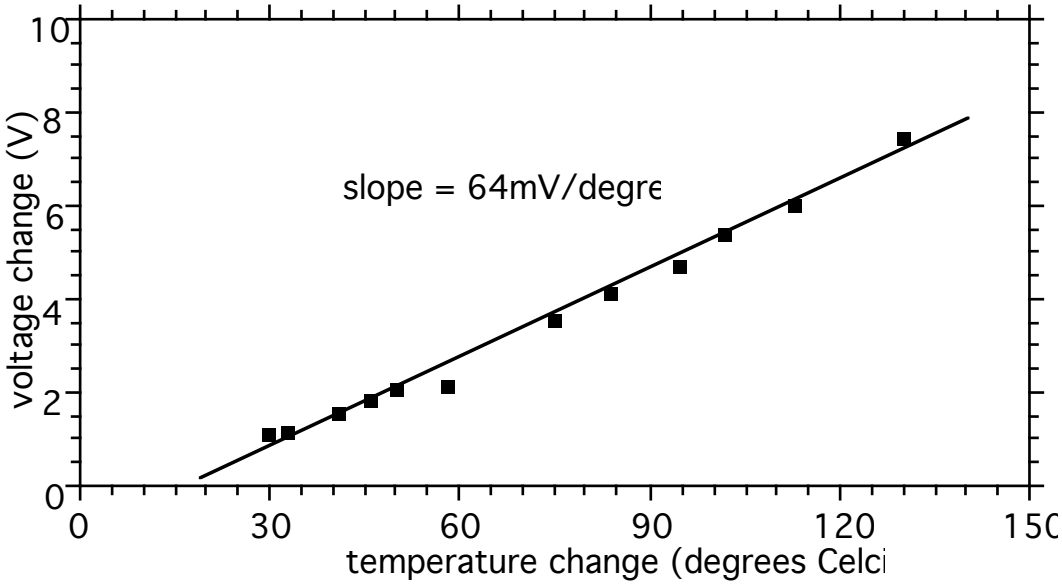

Figure 3.7: Calibration curve of photothermal radiometer with aperture 5 mm away from tube. Saturation occurred at 140°C.

T is surface temperature of the tissue, μ_a is absorption coefficient, E is radiant exposure and ρc is the heat capacity of water. The peak temperature increases are shown in Figure 3.9 and laser exposures are given in Table 2.2.

A comparison between different spot sizes yielded different temperature increases (Figure 3.10). If the slope is assumed to pass through the origin, the slope of the larger condenser is almost twice as large as that of the smaller condenser. This could be due to stain variability. Another example of the variation between samples is shown in Figure 3.11. An experiment conducted on different days for the same condenser yielded slopes that varied by a factor of two.

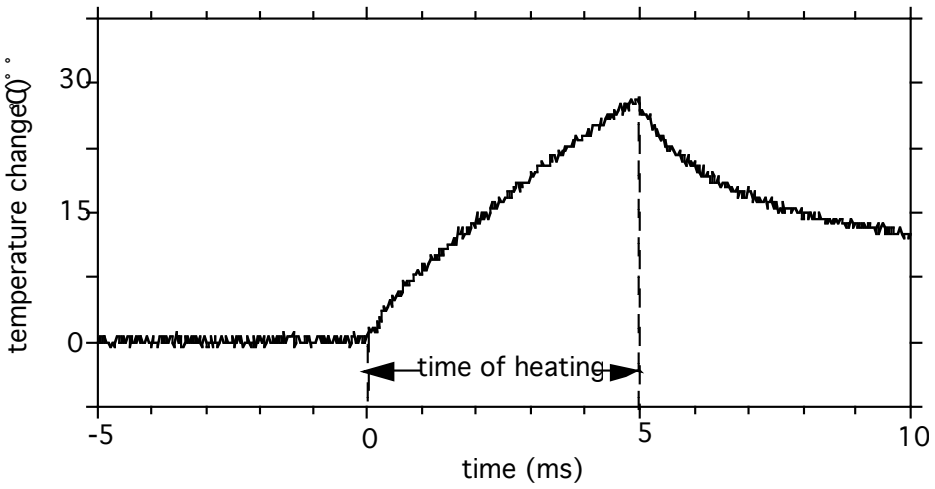

Figure 3.8: Thermal response of stained aorta to a single pulse using 51 mJ/mm^2 and the 6×6 mm condenser. A 30 degree rise in temperature was measured.

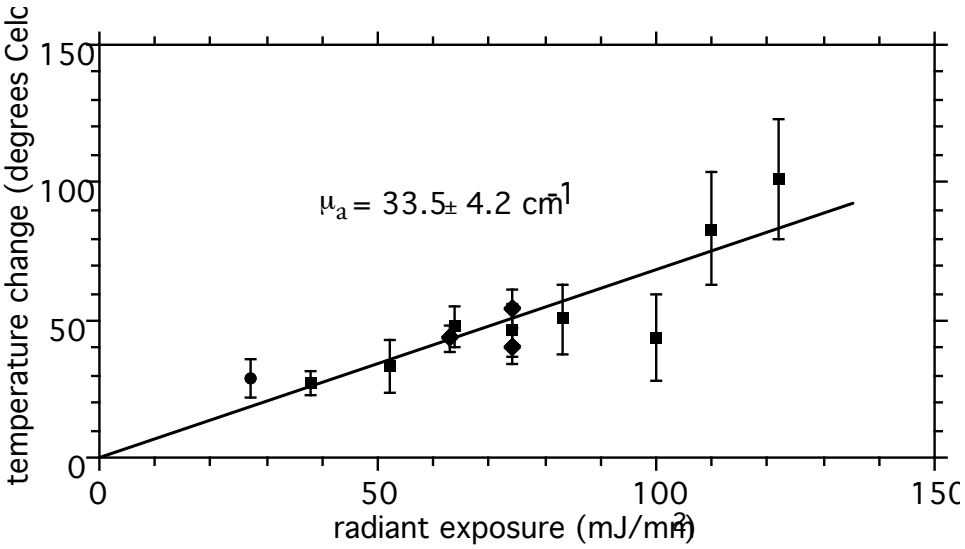

Figure 3.9: Graph of average temperatures for various pulse energies and pulse lengths using the 3×3 mm condenser. Squares, diamonds, and circles are 5, 3, and 1 ms pulse durations respectively.

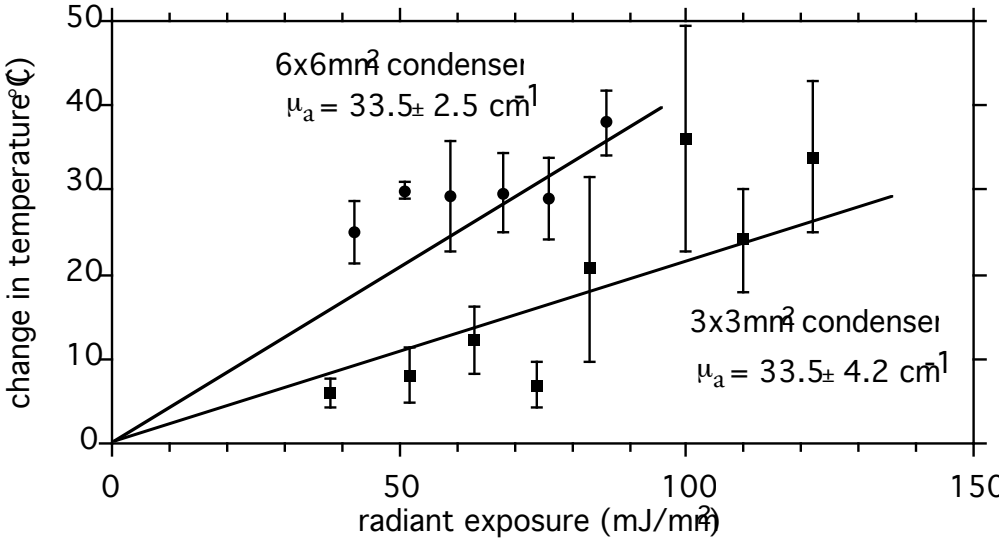

Figure 3.10: Thermal change as a function of radiant exposures for 3×3 mm and 6×6 mm condensers. Illustrates variable heating for different stains of ICG on different aortas. For 6×6 mm condenser data, the best fit line was forced to pass through the origin.

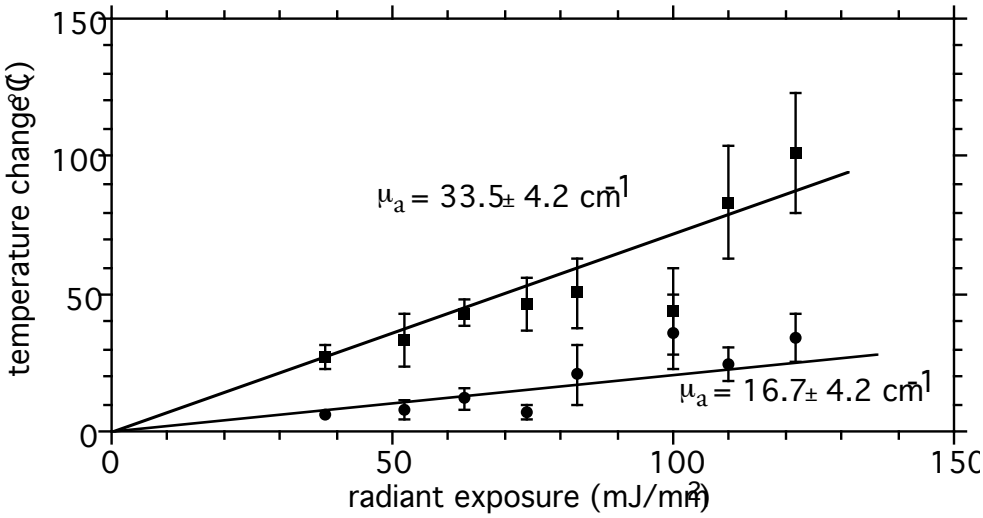

Figure 3.11: A comparison of two different samples using the same spot size. Illustrates sample variation. The samples were prepared from two different aortas.

3.6 Simultaneous Transmission and Thermal Measurements

A typical oscilloscope reading taken after one pulse is shown in Figure 3.12. The transmission data is similar to earlier experiments. The same increase in transmission corresponding to visual bleaching was noted. The transmission through the aorta after one pulse was around 40% and increased to a maximum of around 80% when bleaching was present. Because transmission increased with successive pulses, indicating a decrease in absorption coefficient, a corresponding decrease in temperature was expected. However, this was not observed. Temperature remained constant over several pulses. See Figure 3.13 and Figure 3.14

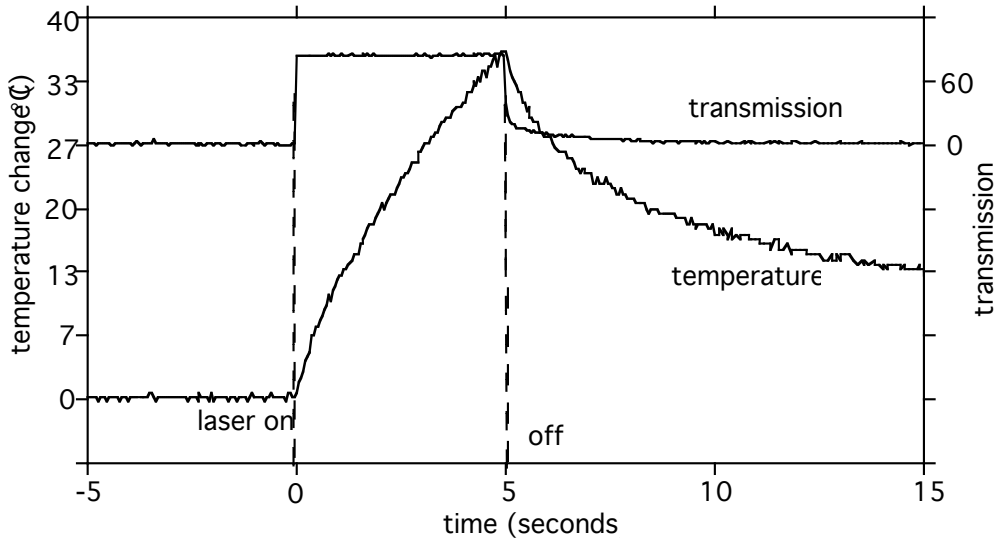

Figure 3.12: Oscilloscope reading of thermal detector and photodiode, showing simultaneous bleaching and thermal measurements. The laser was set to a 59 mJ/mm^2 radiant exposure.

Repeated measurements at 97 mJ/mm^2 yielded similar results (Figure 3.15).

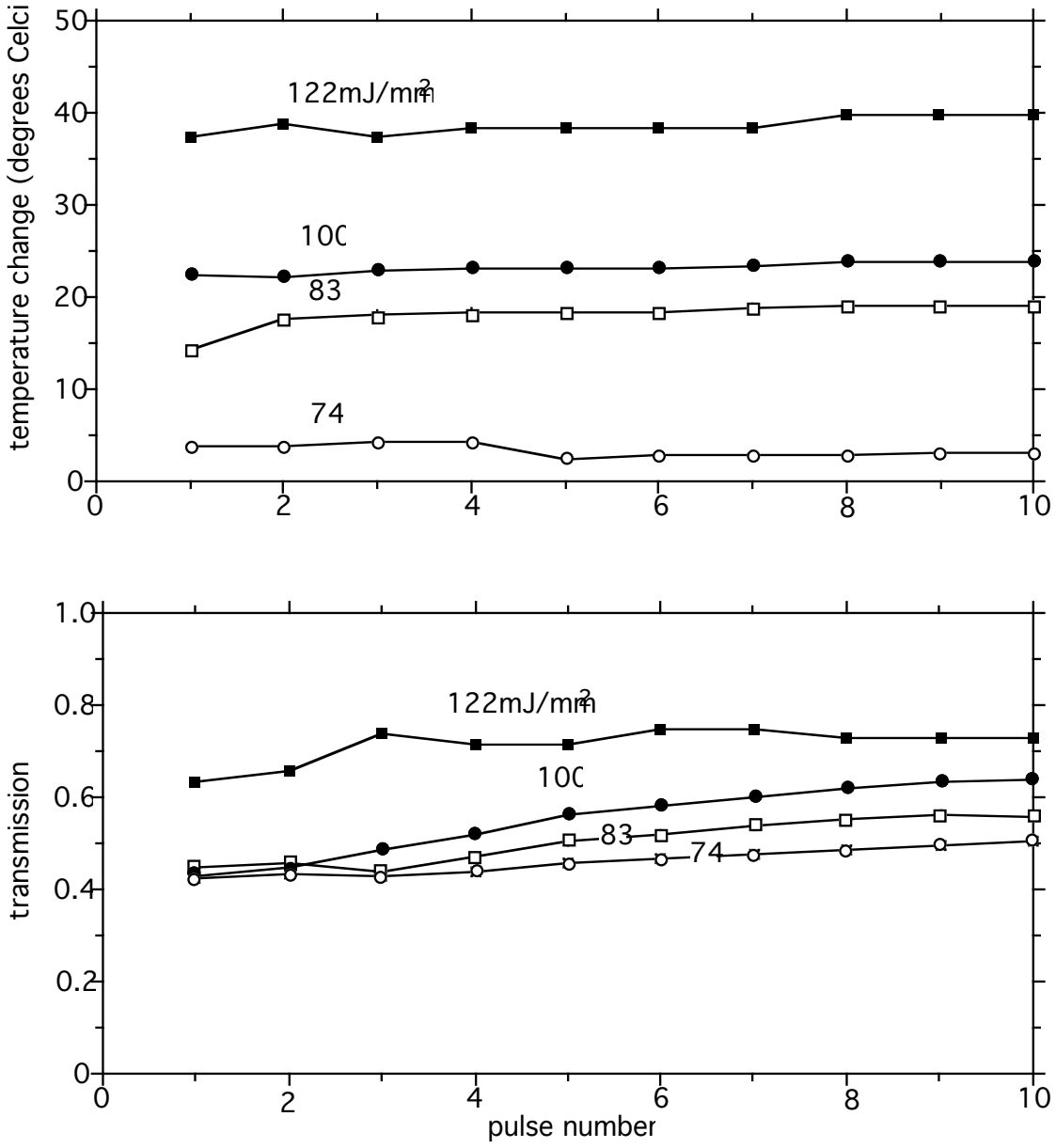

Figure 3.13: A comparison of temperature and transmission measurements using the 3×3 mm condenser. Temperature was constant with successive pulses. Transmission increased with successive pulses at high radiant exposures.

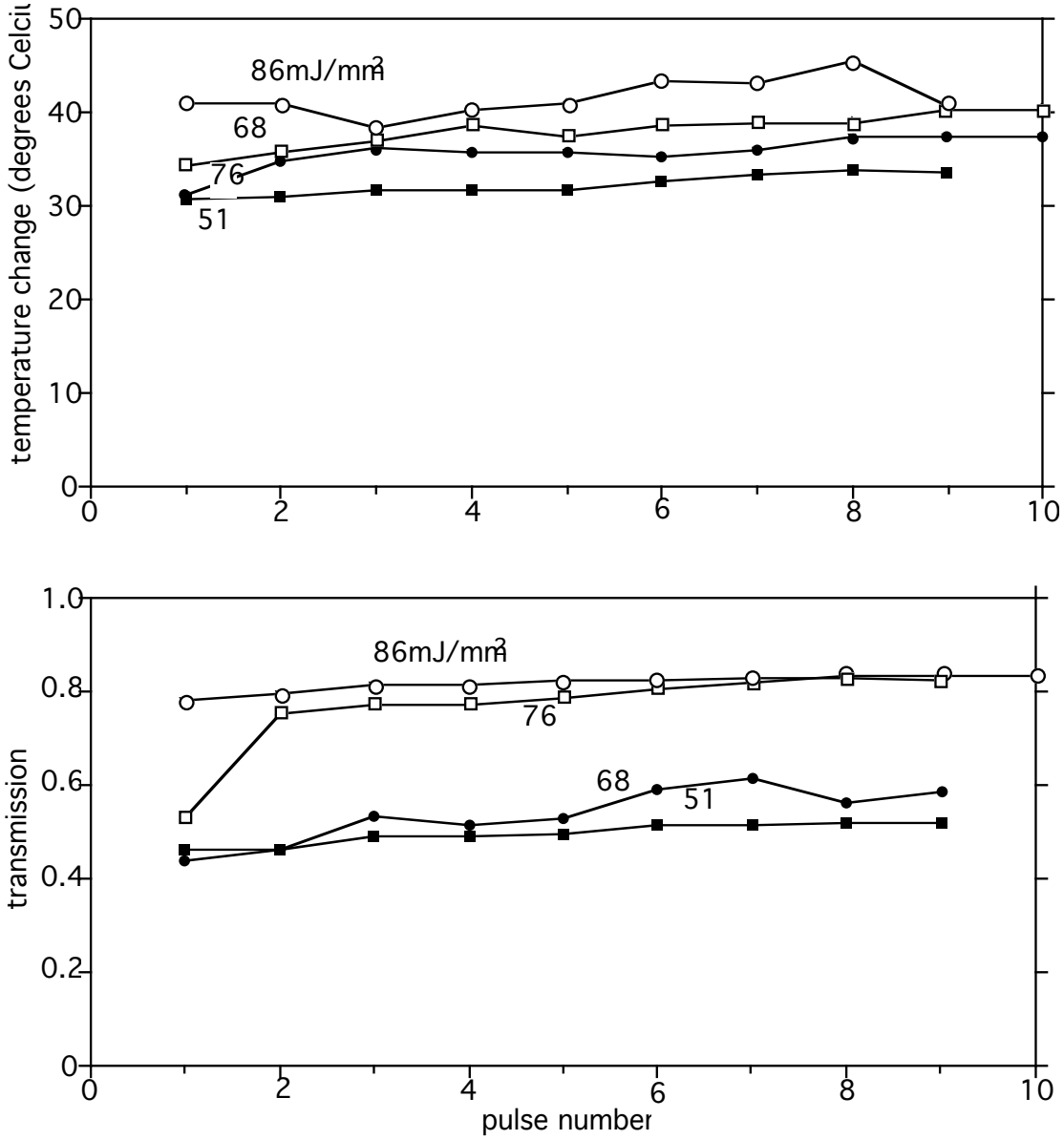

Figure 3.14: A comparison of temperature and transmission measurements using the 6×6 mm condenser. Temperature was constant with successive pulses. Transmission increased with successive pulses at high radiant exposures.

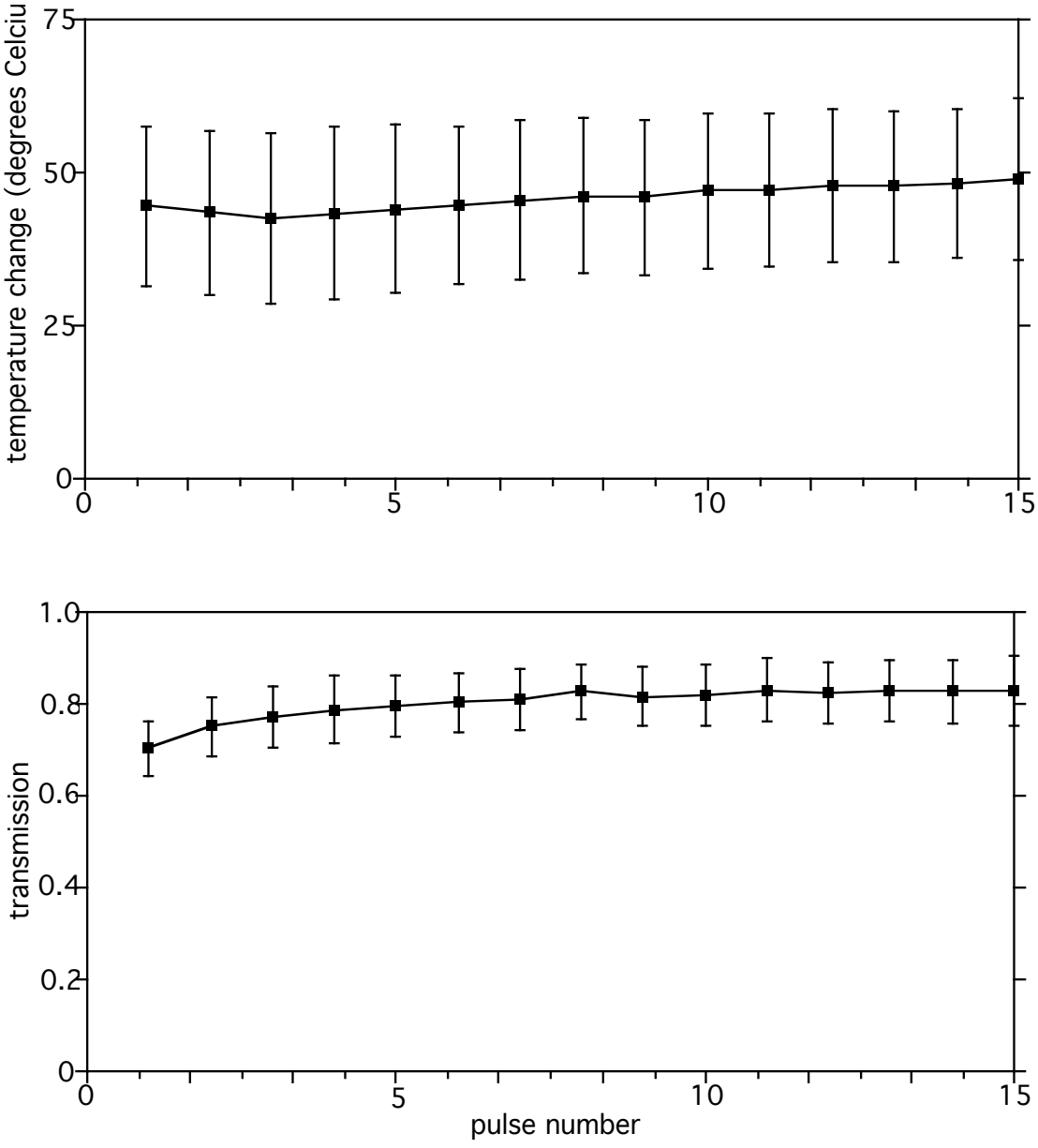

Figure 3.15: Temperature and transmission measurements at $97\,\mathrm{mJ/mm^2}$ for repeated experiments. The temperature remained constant over several pulses while transmission increased over the first five pulses. Error bars represent standard error of the mean.

3.7 Welding

3.7.1 Welding without Pressure

For welds attempted between stained aorta and unstained biomaterial, no welds were made, but faint bleaching of the aorta was noted at both 76 mJ/mm^2 using the 6×6 mm condenser and 74 mJ/mm^2 using the 3×3 mm condenser. Bleaching of the aorta was noted in both cases.

No welds were achieved using biomaterial that was stained on both sides. However, different effects were noted for different pulse trains. At seven pulses at 1 Hz or 2 Hz, the biomaterial bleached orange in one pulse. Twenty successive pulses burned a hole straight through the material causing a bright orange bleach on the aorta. ICG splattered and steam erupted with each pulse.

For welds attempted with biomaterial stained on one side and unstained aorta, no welds were made. However, there was an interesting effect of the laser light on the stained layer of biomaterial. Depressions or gaps were made in the biomaterial where the laser was fired. The ICG at that spot was gone, leaving behind faint bleaching (Figure 3.16). For the second attempt to weld stained biomaterial to unstained aorta, very weak welds were achieved after 7–10 pulses, mostly along the edge of the biomaterial.

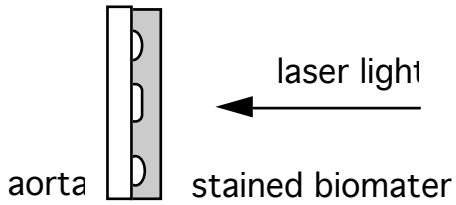

Figure 3.16: Attempted weld between unstained aorta and stained biomaterial on inner side. No was weld made, but instead depressions were formed in biomaterial at weld sites.

Some attempts were made to measure the transmission of the sample as welding occurred, but this was logistically difficult. Figure 3.17 shows the lack of change in transmission when welds were attempted using two pulse energies with the 6×6 mm condenser without any pressure. No visual bleaching occurred, verifying our transmission result.

3.7.2 Welding with Pressure

Welds were successfully achieved when sufficient pressure was used. Pressures greater than 5 N/cm^2 were needed to achieve a minimum weld. A weak weld was defined as stickiness just at

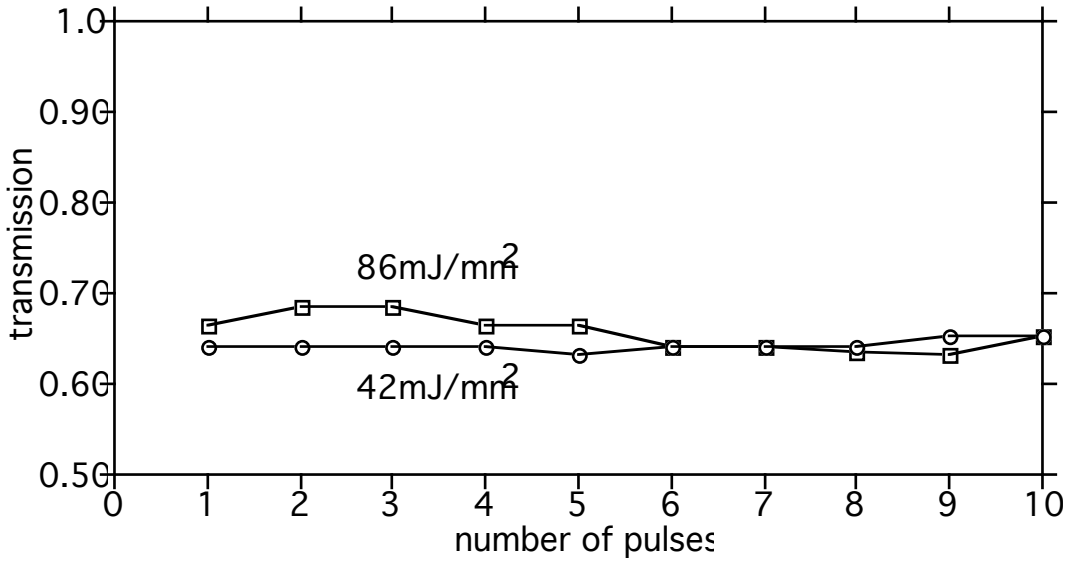

Figure 3.17: Transmission of attempted weld without pressure between stained aorta and unstained biomaterial. No weld made, no bleaching noted.

the corners of the sample. A medium weld was defined as stickiness over the entire sample. A strong weld was stickiness over the entire sample, and corners of biomaterial remained behind after weld was pulled apart. An extremely strong weld was defined as the biomaterial ripping before weld was pulled apart at all places on the sample. Results are shown below in Table 3.18.

Under the microscope, the welds were extremely well formed. The stained layer was very distinct, the interface between biomaterial and weld was easily apparent and uniform—there was no significant destruction of either biomaterial or aorta at the interface. Instead, there was a smooth connection between surfaces.

From experiments in which the biomaterial was squeezed before welding, it was determined that pressure was necessary for strong welds, water content effected weld strength. Furthermore, it is better to apply pressure and weld simultaneously than apply pressure before welding.

Table 3.4: Parameters for welding with pressure. A weak weld was defined as stickiness just at the corners of the sample. A medium weld was defined as stickiness over the entire sample. A strong weld was stickiness over the entire sample, and corners of biomaterial remained behind after the weld was pulled apart. An extremely strong weld was defined as the biomaterial ripping before the weld was pulled apart at all places on the sample.

Pressure (N/cm^2)	Area (cm^2)	Weight (kg)	Weld Strength
4.8	3.06	1.5	*no weld*
5.0	1.95	1.0	*very weak*
6.3	1.87	1.2	*medium*
8.9	1.32	1.2	*medium*
11.6	1.69	2.0	*extremely strong*
11.7	1.68	2.0	*medium*
12.6	1.56	2.0	*strong*
14.8	1.32	2.0	*strong*
19.6	1.00	2.0	*strong*

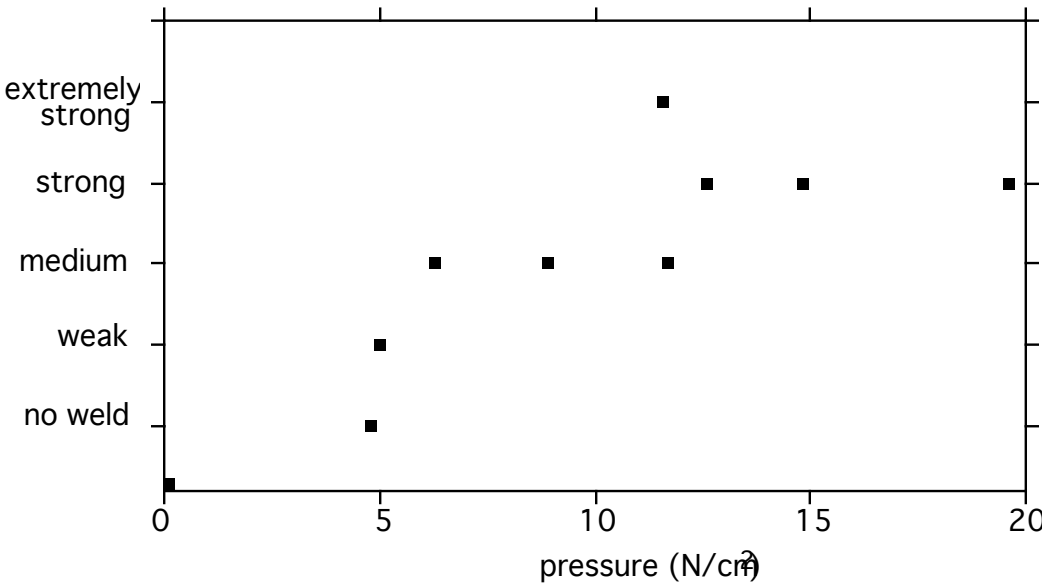

Figure 3.18: Welding with pressure. Strong welds made (the corners of the biomaterial remained attached to the aorta after pulling apart the weld) using pressures above $\sim 12\,N/cm^2$

Chapter 4

Discussion

4.1 Biomaterial

The elastin-based biomaterial was strong, elastic, and nearly transparent to 808 nm laser light. Various methods of improving the material, such as the addition of fibronectin and factor XIII have been shown to increase the strength of biomaterial, and may be used in future experiments [22]. However, material consisting of only fibrinogen, elastin and collagen was sufficiently strong for preliminary welding experiments. Staining the homogeneous biomaterial may be a better method of delivering light absorbing chromophore to the tissue, since uniformly staining aorta was difficult. Because ICG is highly absorbing and the biomaterial is 1 mm thick in these studies, a stained section of biomaterial may absorb most of the laser light before the light reaches the weld site. Therefore, a thin layer of stained biomaterial or biomaterial stained on just one side is probably necessary. Future use of elastin-based biomaterial for welding is promising.

4.2 Steady-State Thermal Measurements

Water bath welds are useful for isolating the thermal conditions necessary for laser welding. Once the temperature requirements for steady-state welds were determined, reproducing those temperatures at a laser weld site was attempted.

4.2.1 Thermal Tests

The first thermal tests showed that the biomaterial did not significantly change until over 100°C. The only significant change—bubble formation on the biomaterial surface—occurred at temperatures greater than 60°C. Sixty degrees centigrade was chosen as the lowest temperature for attempting water bath welds. The biomaterial did not lose its shape, strength, or elasticity, and

showed no evidence of denaturation except at temperatures well above 100°C after heating and cooling. Therefore the biomaterial was considered thermally stable for welding.

4.2.2 Biomaterial to Porcine Aorta Welds

Anderson *et al.* proposed that the mechanism of laser welding involves the conversion of loose collagen fibril ends to a glue upon heating [14]. These assumptions indicate that temperature and tissue contact are important factors for producing welds. Experimental results confirmed this. A temperature of at least 65°C for 5 minutes in a water bath is required for a strong weld, and welds did not occur unless pressure was applied. Pressure alone does not result in a weld.

Results indicate that the biomaterial-aorta interface must reach at least 65°C to achieve a weld, and that good contact, including pressure, is required for laser welding. This is consistent with results by others who have had successful welds within this temperature range and who have applied pressure in some cases [9, 13].

4.3 Penetration Depth of Indocyanine Green

Indocyanine Green (ICG) is known to bind to proteins such as albumin and collagen [28]. ICG delivery to the aorta was accomplished in three ways: in a saturated solution in water, in a 25% albumin (blood protein) mixture, and in a healon glue. The albumin and glue samples yielded a grainy stain on the tissue, and the ICG in water was more uniform. The graininess may arise because the ICG already has bound to the proteins in the first two solutions, and only small amounts of unbound ICG was left to bind to proteins in the tissue. Because water yielded a more uniform stain, a saturated solution of ICG in water was the standard method of applying ICG to aorta. The depth of ICG staining in the aorta was measured to be approximately 200 μm.

ICG undergoes a shift in absorption from 774 nm to 805 nm in solutions of human serum albumin [7]. It remains unclear if these same shifts occur when ICG is bound to aorta.

Evidence of ICG uptake by aorta can be seen in Figure 4.1. A small amount of ICG saturated in water was placed on the intimal side of aorta. A drop of ICG left over from staining tissue was collected at 30 seconds and at 5 minutes after exposure to the aorta surface, placed between glass slides, and an absorbance spectra taken. The 700 nm absorption peak decreases dramatically within a few minutes. This indicates that ICG is binding to the tissue within minutes, leaving a more dilute solution behind. Figure 4.2 shows the absorption peak in detail. The shift of absorption is occurring in tissue since temperature sufficient for welding only occurs when ICG

is present in the tissue.

It was later discovered that ICG has a different absorption peak depending on concentration [28]. At low concentrations the peak is at ∼775 nm. At saturation, the peak is at 700 nm. As can be seen in Figure 4.3, in the less concentrated solution, both the 700 nm peak and the 775 nm peak are present. At high concentrations, the 700 nm peak is predominant, with just a small shoulder at around 774 nm. This change in peak absorption was not immediately noted because the saturated ICG solution was diluted for measurement with the spectrophotometer. When a drop of saturated solution at 5 mg/ml was placed between glass slides, and a spectra taken, the predominance of the 700 nm absorbance peak was noted. This belated discovery, which was already well known in literature, may mean that applying saturated solutions to aorta in the attempt to achieve a deeper stain in fact means not taking advantage of the desired 774 nm absorption peak of ICG. Using a dilute solution of less than 0.5 mg/ml may yield a higher absorbance at the laser wavelength, and consequently better heating and welds [28].

.

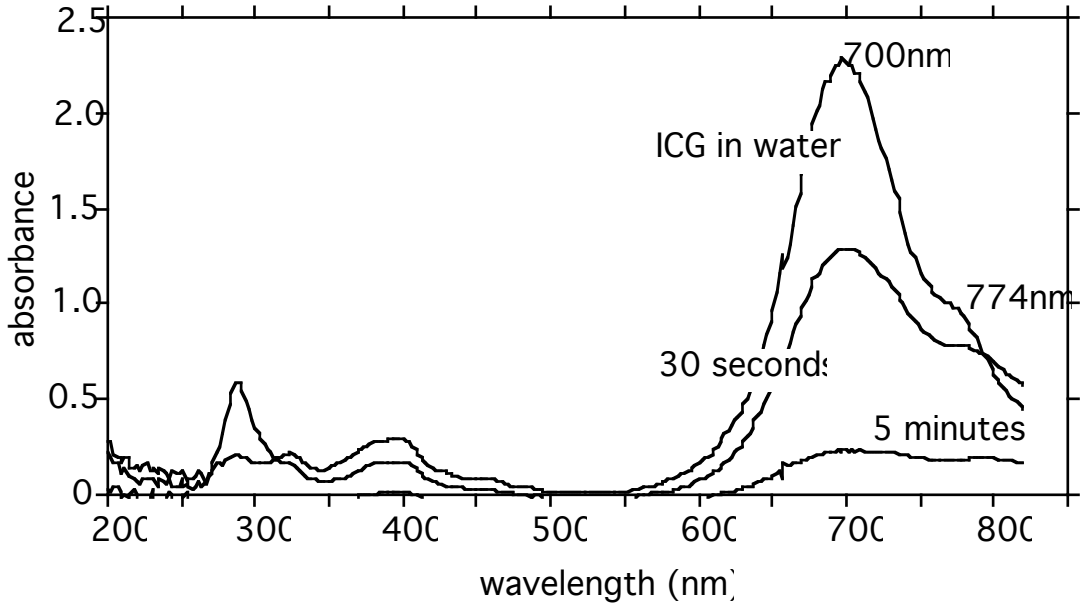

Figure 4.1: The change in absorption of ICG in water after exposure to tissue surface. A less concentrated solution of ICG remained on the tissue surface as ICG is taken into the tissue over a period of minutes.

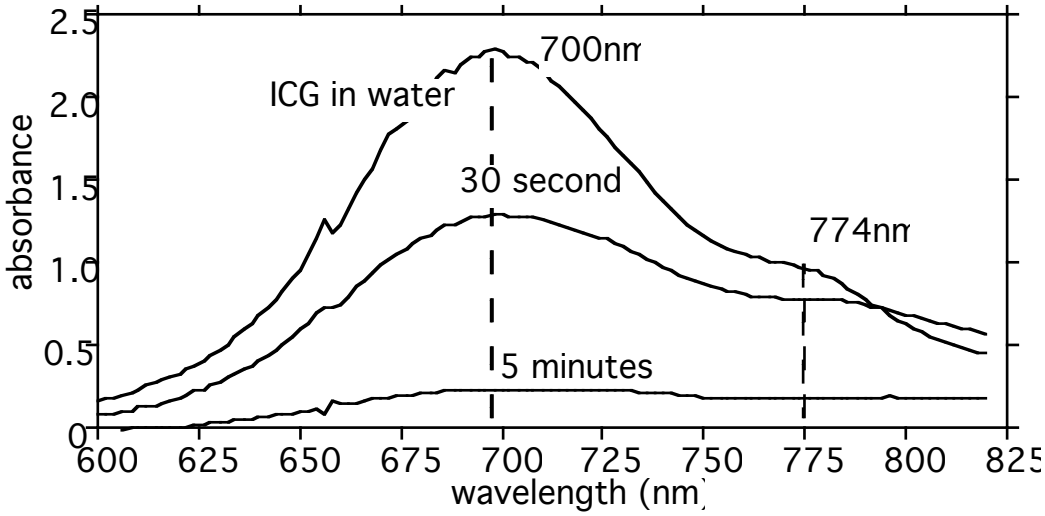

Figure 4.2: The change in absorption of ICG in water after exposure to tissue surface. A less concentrated solution of ICG remained on the tissue surface as ICG is taken into the tissue over a period of minutes.

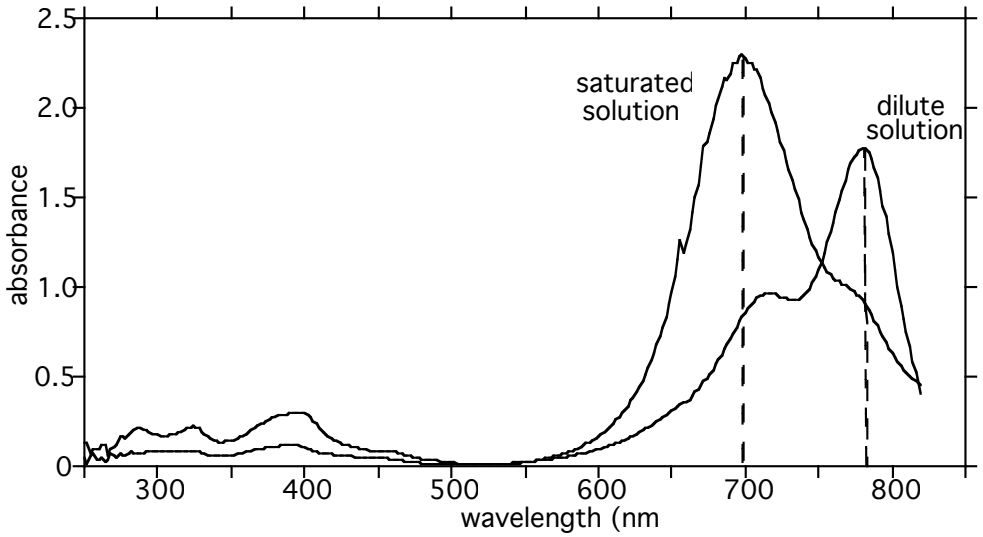

Figure 4.3: A comparison of absorption spectra for saturated and dilute solutions of ICG. The saturated solution was 5 mg/ml, dilute solution less than 0.5 mg/ml. ICG has two absorption peaks. The prominence of these peaks depends on concentration.

4.4 ICG Transmission Measurements

According to transmission measurements the absorption coefficient of aorta increases from $\sim$0.5cm^{-1} to $\sim$35cm^{-1} after ICG is added. This coefficient can be found by taking transmission measurements of the stained tissue if the penetration depth of ICG is known. The penetration depth is assumed to be uniform, however, it varied between 100 and 400 μm. A simple approximations for the transmission through a stained aorta sample is:

$$T = T_o \exp(-\mu_a d)$$

therefore,

$$\mu_a = \frac{-\ln T/T_o}{d}$$

where T is transmission of the stained aorta, T_o is the transmission of the unstained aorta, d is the thickness of the stained layer, and μ_a is the absorption coefficient. Looking at the 84 mJ/mm^2 radiant exposure, transmission began at 50% and reached a maximum of 80% over a series of pulses. The corresponding μ_a range was from 35–11cm^{-1}.

Bleaching seems to depend on the number of pulses and the radiant exposure. If the radiant exposure is low, it takes several pulses for bleaching to occur. At the lowest radiant exposures, no bleaching is seen. At higher radiant exposures, bleaching occurs within a few pulses. From looking at a plot of radiant exposure versus pulse number at maximum bleaching, a curve for bleaching can be seen, with faint bleaching occurring below the curve and no bleaching occurring to the left of the curve (Figure 4.4). Maximum bleaching was defined to occur at the pulse number at which no increase in transmission is observed.

At low energies, no bleaching or change in transmission was noted, and transmission through the layer was around 50%. At higher energies transmission increased with successive pulses until a maximum was reached. At the highest energies bleaching occurred within one or two pulses and transmission remained at the maximum level of 80-85%. It is possible that the ICG is being chemically changed, and the effectiveness of the ICG for increasing heating at the stained area is slowly decreasing, resulting in a lower effective penetration depth with each pulse. Support for this hypothesis is discussed in the following sections. At low radiant exposures insufficient energy is delivered, effecting no change in ICG. At mid-range energies each pulse has enough energy to change the ICG's absorption, and since there is less effective ICG to absorb the light,

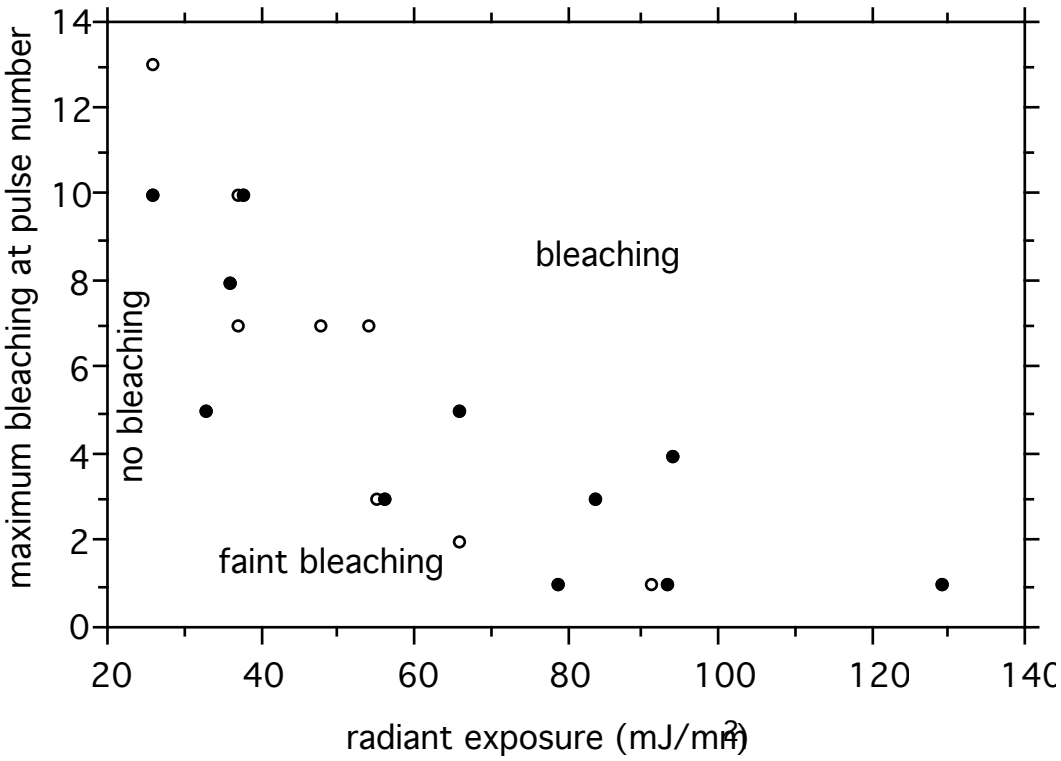

Figure 4.4: Threshold for maximum bleaching as a function of pulse number. Filled circles are measurements taken with the 3×3 mm condenser, and unfilled circles with the 6×6 mm condenser. Bleaching depends on the number of repetitive pulses. With higher radiant exposures, bleaching occurs in the first few pulses. At lower radiant exposures, bleaching occurs over several pulses. At low radiant exposures, no bleaching is observed, even with multiple pulses.

transmission through the sample increases. It takes several pulses at this radiant exposure to completely bleach the ICG. At highest radiant exposures there is enough light to change the ICG within one or two pulses. Therefore, transmission remains high over several pulses, and no increase is seen.

It was unknown if ICG underwent a thermally induced change when exposed to heat. However, Dimitrov *et al.* reported that hours of exposure to temperatures higher than needed for laser welding were required to see any decrease in absorbance, and there was no shift in peak absorption [29]. Therefore, the bleaching effect noted when ICG is exposed to laser light is not due to heating, but most likely a photochemical phenomenon. However, these experiments should be repeated to verify that there is no thermal change for high concentrations of ICG.

4.5 Thermal Measurements

From transmission experiments the ICG layer was expected to be effective for confining heat and aiding welding, at least until the ICG is completely bleached. Thermal measurements of the ICG layer were carried out to confirm temperature calculations from transmission measurements.

The temperature model assumes uniform thermal properties equal to those for water, since tissue is mostly composed of water. Temperature is related to μ_a by the following equation:

$$T = \frac{\mu_a E}{\rho c}$$

where T is temperature, μ_a is absorption coefficient, E is radiant exposure, and ρc is the heat capacity of water. From this equation, μ_a can be calculated once the temperature is measured. A comparison of the μ_a calculated from transmission and temperature experiments is given below. For a radiant exposure of $84\,\mathrm{mJ/mm^2}$, μ_a was calculated to be $35\mathrm{cm}^{-1}$. Using this absorption coefficient, a temperature increase of 70°C is expected. However, at $83\,\mathrm{mJ/mm^2}$ the temperature change was measured to be around 50°C, yielding a μ_a of $25\mathrm{cm}^{-1}$. This 20 degree discrepancy is probably due to the variability of staining between samples. Simultaneous measurements of transmission and temperature were made to eliminate sample variability.

As expected, temperature was proportional to radiant exposure. Temperature increases up to 100°C were observed. Since water bath welds suggested that 65°C for five minutes in a waterbath was enough to achieve a weld, successful welding at these exposures was anticipated. It is assumed that five minutes were required for the sample to reach 65°C. Also, different pulse lengths at the

same radiant exposure yielded the same increase in temperature, confirming that pulsed laser welding does not depend on pulse length as measured in this experiment (Figure 3.9).

Comparing single pulse measurements done on different days, there were a significant differences in heating. One experiment yielded temperature increases of over 100°C while another experiment showed increases no greater than 50°C. This was almost certainly due to variations of ICG concentration in the tissue.

4.6 Simultaneous Transmission and Thermal Measurements

Simultaneous measurements were conducted over a range of radiant exposures. Surface temperatures remained constant over a series of pulses at all radiant exposures instead of decreasing as expected with the measured increase in transmission (Figure 4.5).

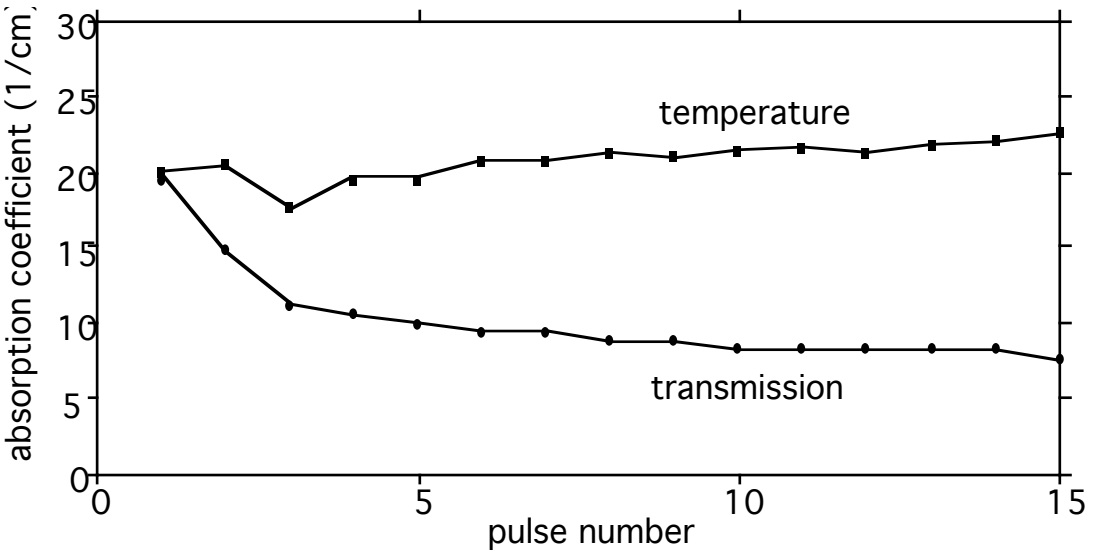

Figure 4.5: The calculated absorption coefficients from transmission and thermal measurements over a series of pulses at 97 mJ/mm^2. The absorption coefficient calculated from thermal measurements indicated that the concentration of ICG in aorta remained constant at the surface. The absorption coefficient calculated from transmission measurements indicated that the effective ICG depth was changing with repetitive pulses.

To verify this unexpected observation, this experiment was repeated several times at 97 mJ/mm^2 using different sections of the same aorta. Similar results were observed. Dehydration of the tissue would cause temperature to rise, however neither dehydration nor a rise in temperature was observed. If transmission and temperature observations are assumed real, then a change in the

depth of penetration with bleaching is the only other factor left in the experimental model to explain the discrepancy between calculated absorption coefficients. From bleaching measurements, it was postulated that the effectiveness of the ICG, or the effective depth, was changing with each pulse. The changing effective ICG depth with pulses was calculated as follows. The equation for temperature was used to obtain the absorption coefficient.

$$\mu_a = \frac{T\rho c}{E}$$

When this value for μ_a is substituted into the transmission equation then the following relation for the effective ICG depth d is obtained.

$$d = \frac{-\ln(T/T_o)}{\mu_a}$$

Figure 4.6 shows the relationship between d and the number of repetitive pulses. Notice that the calculated exponent is for one run of the experiment.

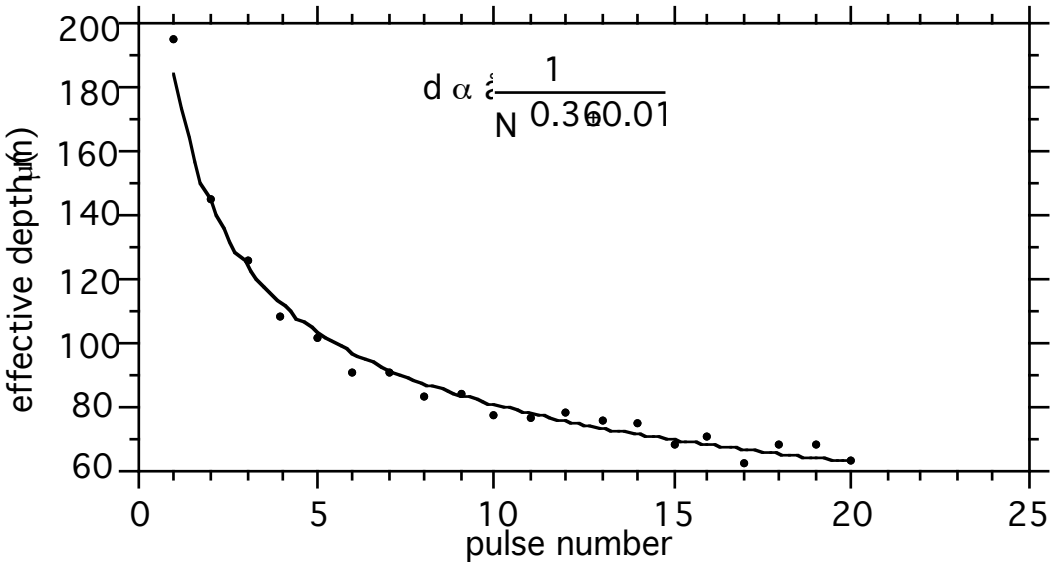

Figure 4.6: The effective ICG depth versus pulse number for one sample. N is the number of pulses. The calculated exponent for this run is -0.36. Radiant exposure was 9.7 mJ/mm^2 using the 4×4 mm condenser.

To determine an estimate for the relation between ICG depth and pulse number, the exponent and its standard deviation were calculated for each run of the experiment. The exponent was the power that the pulse number was raised. For the experiment shown in Figure 4.7, the exponent

was -0.36. The effective depth of ICG was found to be inversely proportional to the fourth root of the pulse number after calculating a weighted value from all runs of the experiment, including those done at different radiant exposures. The following equations were used to calculate the weighted exponent:

$$\mu = \frac{\sum(x_i/\sigma_i^2)}{\sum(1/\sigma_i^2)}$$

$$\sigma_\mu^2 = \frac{1}{\sum(1/\sigma_i^2)}$$

where μ is the mean value calculated for the exponent, x_i is the exponent for each run, σ_i is the standard deviation for each exponent, and σ_μ is the uncertainty of the mean for the exponent. Figure 4.7 includes the calculated exponent for each run of the experiment. The dashed lines represent the average of these exponents, and weighted mean.

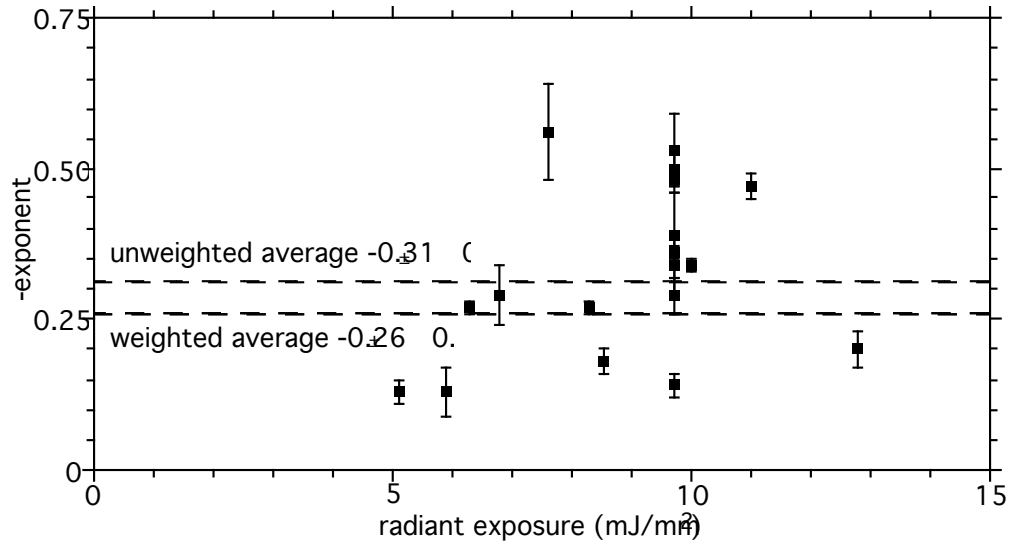

Figure 4.7: Calculated exponent for each experiment. A weighted fit of all the experiments yielded an exponent of -0.25. The unweighted exponent was -0.31 An exponent of -0.25 has been observed in other studies on the depth of tissue damage over repetitive laser pulses.

Why this should be so is unclear. However, at least four others have also seen this relationship when studying the depth of ocular damage over repetitive pulses of medical lasers [30]. This experiment shows the change in the effective ICG depth, and not damage to the aorta. The multiple appearance of these results suggests a basic relationship for repetitive laser pulses and depth of damage. Because the experiment for studying the effective ICG depth is relatively

simple compared to the other studies of the depth of ocular damage, it may be possible to derive a theoretical model to explain why the depth of damage or effective ICG depth is inversely proportional to the fourth root of the pulse number. To date no explanation has been derived to explain this phenomenon.

4.7 Welding

A radiant exposure high enough for maximum bleaching over 4–5 pulses using the 3×3 mm condenser was used to weld aorta to biomaterial to ensure enough energy delivered within a few pulses. Welds without pressure were unsuccessful. It is important to note that no welds were achieved at any energy without ICG.

Bleaching of either the aorta or the biomaterial was often observed around the edges of our welding sample. Welds were strongest in these areas. This is probably because light did not have to pass through the biomaterial at the edges, and more heating was induced at these places on the sample. In the absence of sufficient pressure welding was not successful regardless of bleaching. Bleaching may indicate when enough light has reached that particular area, and when the operator may move to the next area to be welded.

In later experiments it was noticed that the more dehydrated the biomaterial, the less pressure was needed for a successful weld. One possible explanation is that squeezing out the water allows for better contact between biomaterial and aorta. Another possibility is that removing the water reduces the heat capacity and therefore the sample reaches a higher temperature. The layer of stained aorta was distinct when viewed under the microscope after welding. In fact, in some cases this layer could be peeled away before and after welding. It is not clear if this was due to dehydration of the aorta, or an effect of the ICG on the intimal layer in which the staining process physically separates the layer from the rest of the aorta.

4.8 Recommendations for Further Studies

Several unknowns remain. The first is the anomalous surface temperatures measured by the photothermal radiometer. Although differences in measured temperatures for different aortas are probably due to variability of ICG staining, measurements using thermocouples should to be attempted to verify these results.

The most complicated variable is ICG staining. So far it has been determined that the ICG

absorption peak depends on concentration, light exposure, and solvent used. It is still unclear if ICG undergoes a shift in absorption peak when bound to tissue. Optical measurements to determine concentration and absorption spectra are vital in controlling these variables. The use of an optical multichannel analyzer to measure the absorbance spectra reflected from the stained tissue surface may be possible.

The mechanism for biomaterial/aorta welding is still unknown. More thermal measurements to isolate the mechanism are required. Welds between biomaterial and welds between tissue may isolate the temperatures, and possibly the extracellular proteins responsible for welding. Studies in this thesis only determined a threshold temperature for welding. It is entirely possible that weld strength may vary over a temperature range. The upper boundary still needs to be established.

Welding is possible between biomaterial and aorta. The best results were achieved with at least $12\,\mathrm{N/cm^2}$ of pressure when using the $3{\times}3\,\mathrm{mm}$ condenser at $86\,\mathrm{mJ/mm^2}$. The intimal side of the tissue should be stained for 5 minutes using a saturated solution of ICG in water. Better heating may be achieved using an ICG concentrations less than $0.5\,\mathrm{mg/ml}$ [28].

4.9 Summary

Conclusions may be drawn from this initial study of ICG dye-enhanced tissue welding of elastin-based-biomaterial. First, steady-state thermal welds show that the biomaterial is thermally stable throughout the range of temperatures required for laser welding. At least 65°C and $5\,\mathrm{N/mm^2}$ are required to achieve a weld between biomaterial and aorta. These requirements are comparable to previous collagen welding studies. The biomaterial does not contain a large amount of collagen in comparison with fibrin and elastin. Additionally, the biomaterial is thermally stable to 100°C. Therefore, it is likely that thermal changes responsible for welding are occurring on the aorta side of the aorta/biomaterial interface. The intimal side of aorta does have collagen present. The mechanism for welding biomaterial to aorta could be a melting of collagen on the aorta, causing a glue to form and adhere to the biomaterial. The aorta used is dead tissue, and proteolytic degradation has taken place. This may explain why cutting collagen fibers, as Anderson did in his welding experiments, is not necessary [14].

The staining of tissue with ICG is complicated. Using ICG in solution of blood protein yields an inferior stain compared to staining with ICG in water. The penetration depth of ICG into aorta is $\sim 200\,\mu\mathrm{m}$. However, these measurements were done using a saturated solution of ICG,

which is shown to have a peak absorption at 700 nm. These measurements should be repeated using a less concentrated solution.

Bleaching of ICG occurs when exposed to radiant exposures of above $\sim$25 mJ/mm^2, indicating that bleaching is a threshold effect. Transmission measurements steadily increase to a maximum, indicating that the absorption coefficient of the stained layer is decreasing with repetitive pulses.

Thermal measurements of the surface of stained aorta show temperatures sufficiently high for welding. Also, there is a proportional relationship between radiant exposure and temperature as predicted by a simple thermal model. A radiant exposure twice as large yields a temperature twice as large. There is considerable difference in heating between different samples and different spot sizes, which is most likely the result of variable ICG uptake.

Simultaneous transmission and thermal measurements of ICG yielded a relationship between the depth of penetration and the number of pulses. The depth of penetration was inversely proportional to the fourth root of the number of pulses. This relation between depth and pulse number was seen in other studies of ocular damage due to repetitive pulses. The reasons for this effect have yet to be determined. The calculated penetration depth at the first pulse was about 180 μm.

Dehydration of the biomaterial may play a role in decreasing the laser energy needed for welding. Laser welding attempts were successful only when ICG was present. Pressures of 5 N/cm^2 at 86 mJ/mm^2 were required for a minimum weld between aorta and biomaterial.

Dye enhanced laser welding of aorta and biomaterial proved to be an extremely complicated problem. However, once the behavior and concentration of ICG in tissue is understood, and induced heating is predictable and reproducible, pulsed diode laser welding shows promise of being a viable method for wound closure and healing.

Bibliography

[1] H. W. Popp, M. C. Oz, L. S. Bass, R. S. Chuck, S. L. Trokel, and M. R. Treat, "Welding of gallbladder tissue with a pulsed 2.15 μm thulium-holmium-chromium:YAG laser," *Lasers in Surg. and Med.*, vol. 9, pp. 155–159, 1989.

[2] J. L. McCue and R. K. S. Phillips, "Sutureless intestinal anastomoses," *Br. J. Surg.*, vol. 78, pp. 1291–1296, 1991.

[3] L. I. Deckelbaum, J. M. Isner, R. F. Donaldson, S. M. Laliberte, R. H. Clarke, and D. N. Salem, "Use of pulsed energy delivery to minimize tissue injury resulting from carbon dioxide laser irradiation of cardiovascular tissues," *J. Am. Coll. Cardiol.*, vol. 7, pp. 898–908, 1986.

[4] L. W. Murray, L. Su, G. E. Kopchok, and R. A. White, "Crosslinking of extracellular matrix proteins: a preliminary report on a possible mechanism of argon laser welding," *Lasers in Surg. and Med.*, vol. 9, pp. 490–496, 1989.

[5] S. Thomsen, J. R. Morris, C. R. Neblett, and J. Mueller, "Tissue welding using a low energy microsurgical CO_2 laser," *Med. Instrumentation*, vol. 21, pp. 231–237, 1987.

[6] R. A. White, R. P. Abergel, R. Lyons, S. R. Klein, G. Kopchok, R. M. Dwyer, and J. Uitto, "Biological effects of laser welding on vascular healing," *Lasers in Surg. and Med.*, vol. 6, pp. 137–141, 1986.

[7] S. D. DeCoste, W. Farinelli, T. Flotte, and R. R. Anderson, "Dye-enhanced laser welding for skin closure," *Lasers in Surgery and Medicine*, vol. 12, pp. 25–32, 1992.

[8] R. A. White, G. Kopchok, S. Peng, R. Fujitani, G. White, S. Klein, and J. Uitto, "Laser vascular welding—how does it work?," *Ann. of Vasc. Surg.*, vol. 1, pp. 461–464, 1986.

[9] R. A. White, G. Kopchok, C. Donayre, G. White, R. Lyons, R. Fujitani, S. R. Klein, and J. Uitto, "Argon laser-welded arteriovenous anastomoses," *J. of Vasc. Surg.*, vol. 6, pp. 447–453, 1987.

[10] S. G. Brooks, S. Ashley, A. A. Gehani, G. A. Davies, J. Fisher, R. C. Kester, and M. R. Rees, "Laser welding for coronary artery anastomosis: techniques, temperature profiles and the role of chromophores," in *Proceedings of Optical Fibers in Medicine*, Proc. SPIE 1201, pp. 99–105, 1990.

[11] R. M. Fujitani, R. A. White, G. E. Kopchok, S. Peng, G. H. White, and S. R. Klein, "Biophysical mechanisms of argon laser-assisted vascular anastomoses," *Current Surg.*, vol. 45, pp. 119–123, 1988.

[12] R. D. Jenkins, I. N. Sinclair, R. Anand, A. G. Kalil Jr., F. J. Schoen, and J. R. Spears, "Laser balloon angioplasty: effect of tissue temperature on weld strength of human postmortem intima-media separations," *Lasers in Surg. and Med.*, vol. 8, pp. 30–39, 1988.

[13] S. Solhpour, E. Weldon, T. E. Foster, and R. R. Anderson, "Mechanism for thermal tissue "welding" (part 1)," *Lasers Surg. and Med.*, vol. S6, p. 56, 1994.

[14] R. R. Anderson, G. M. Lemole, R. Kaplan, S. Solhpour, N. Michaud, and T. Flotte, "Molecular mechanisms of thermal tissue welding," *Lasers Surg. and Med.*, vol. S6, p. 56, 1994.

[15] S. L. Jacques, "Role of tissue optics and pulse duration on tissue effects during high-power laser irradiation," *App. Opt.*, vol. 32, pp. 2447–2454, 1993.

[16] R. S. Chuck, M. C. Oz, T. M. Delohery, J. P. Johnson, L. S. Bass, R. Nowygrod, and M. R. Treat, "Dye-enhanced laser tissue welding," *Lasers in Surg. and Med.*, vol. 9, pp. 471–477, 1989.

[17] M. C. Oz, R. S. Chuck, J. P. Johnson, S. Parangi, L. S. Bass, R. Nowygrod, and M. R. Treat, "Indocyanine green dye-enhanced welding with a diode laser," *Surgical Forum*, vol. 40, pp. 316–318, 1989.

[18] P. E. Grubbs Jr., S. Wang, C. Marini, S. Basu, D. M. Rose, and J. N. Cunningham Jr., "Enhancement of CO_2 laser microvascular anastomoses by fibrin glue," *J. of Surg. Res.*, vol. 45, pp. 112–119, 1988.

[19] L. S. Bass, S. K. Libutti, and A. M. Eaton, "Tissue bonding and sealing composition and method of using the same," *United States Patent*, 5,292,362, 1994.

[20] J. S. Sauer, J. R. Hinshaw, and K. P. McGuire, "The first sutureless, laser-welded end-to-end bowel anastomosis," *Lasers in Surg. and Med.*, vol. 9, pp. 70–73, 1989.

[21] M. Rabaud, F. Lefebvre, M. T. Martin, M. Aprahamian, R. Schmitthaeusler, and J. P. Cazenave, "Adduct formation between soluble fibrin monomers and elastin," *Biomaterials*, vol. 8, pp. 217–222, 1987.

[22] M. Aprahamian, A. Lambert, G. Balboni, F. Lefebvre, R. Schmitthaeusler, C. Damge, and M. Rabaud, "A new reconstituted connective tissue matrix: Preparation, biochemical, structural and mechanical studies," *J. of Biomed. Mat. Res.*, vol. 21, pp. 965–977, 1987.

[23] M. Rabaud, J. Y. Elie, F. Lefebvre, D. Ducassou, P. Mettetal, M. L. Guillou, D. Collet, J. Perissat, D. Fradin, and F. Fontan, "A new biodegradable elastin-fibrin material; Its use in urological, digestive and cardiovascular surgery," *J. of Biomat. Applications*, vol. 7, pp. 20–46, 1992.

[24] D. Fradin, T. Causs, M. Rabaud, A. de Mascarel, and F. Fontan, "Preliminary experimental results of a new resorbably biomaterial as pericardial substitute (letter)," *J. Thorac. Cardiovasc. Surg.*, vol. 105, pp. 364–78, 1993.

[25] J. F. Marescaux, M. Aprahamian, D. Mutter, E. Loza, M. Wilhelm, P. Sonzini, and C. Damge, "Prevention of anastomosis leakage: an artificial connective tissue," *Br. J. Surg.*, vol. 78, pp. 440–444, 1991.

[26] F. Lefebvre, F. Drouillet, A. M. S. de Larclause, M. Aprahamian, D. Midy, L. Bordenave, and M. Rabaud, "Repair of experimental arteriotomy in rabbit aorta using a new resorbable elastin-fibrin biomaterial," *J. of Biomed. Mat. Res.*, vol. 23, pp. 1423–1432, 1989.

[27] M. Riquet, F. Carnot, P. Galliz, D. Callise, F. Lefebvre, and M. Rabaud, "Biocompatibility of elastin-fibrin material in the rat," *Biomaterials*, 1990.

[28] M. L. J. Landsman, G. Kwant, G. A. Mook, and W. G. Zijlstra, "Light-absorbing properties, stability, and spectral stabilization of indocyanine green," *J. Applied Physiology*, vol. 40, pp. 575–583, 1976.

[29] D. Dimitrov, L. S. Bass, and M. R. Treat, "Thermal breakdown properties of indocyanine green," in *Proceedings of Lasers in Surgery: Advanced Characterization, Therapeutics, and Systems V* (R. R. Anderson, ed.), Proc. SPIE 2395, pp. 486–489, 1995.

[30] D. H. Sliney, "Deriving exposure limits," in *Proceedings of Laser Safety, Eyesafe Laser Systems, and Laser Eye Protection*, Proc. SPIE 1207, pp. 2–13, 1990.

Biographical Note

Ms. La Joie was born in Santa Clara, California on May 22, 1969. She attended San Jose State University and earned the degree of B. S. in physics. Her special interest is in biomedical engineering. She is also the recipient of a MARC-Predoctoral Fellowship granted by the National Institutes of Health.